Published in final edited form as:
Cancer Res. 2014 February 15; 74(4): 979–1004. doi:10.1158/0008-5472.CAN-13-2387.

Light In and Sound Out: Emerging Translational Strategies for Photoacoustic Imaging

S. Zackrisson[#1,2], **S.M.W.Y. van de Ven**[#1], and **S.S. Gambhir**[1,*]

[1] Departments of Radiology, Bioengineering, and Department of Materials Science & Engineering. Molecular Imaging Program at Stanford, Stanford University School of Medicine, Stanford, CA, USA

[2] Diagnostic Radiology, Department of Clinical Sciences in Malmö, Lund University, Sweden

[#] These authors contributed equally to this work.

Abstract

Photoacoustic imaging has the potential for real-time molecular imaging at high resolution and deep inside the tissue, using non-ionizing radiation and not necessarily depending on exogenous imaging agents, making this technique very promising for a range of clinical applications. The fact that photoacoustic imaging systems can be made portable and compatible with existing imaging technologies favors clinical translation even more. The breadth of clinical applications in which photoacoustics could play a valuable role include: noninvasive imaging of the breast, sentinel lymph nodes, skin, thyroid, eye, prostate (transrectal), and ovaries (transvaginal); minimally invasive endoscopic imaging of gastrointestinal tract, bladder, and circulating tumor cells (*in vivo* flow cytometry); and intraoperative imaging for assessment of tumor margins and (lymph node) metastases. In this review we describe the basics of photoacoustic imaging and its recent advances in biomedical research, followed by a discussion of strategies for clinical translation of the technique.

Keywords

Photoacoustic Imaging; Molecular Imaging; Optoacoustic imaging; Clinical Translation; Translational Biomedical Research

Introduction

Photoacoustic imaging (PAI), also referred to as optoacoustic imaging, is an emerging new imaging technique with significant promise for biomedical applications. The key strength of photoacoustic imaging is its ability to collect functional and molecular information from most tissues. One of the major advantages of this technique over other imaging modalities is that photoacoustic imaging has the ability to provide tissue information without using an exogenous molecular imaging agent, by making use of endogenous contrast alone. Additional advantages over other imaging modalities are that photoacoustic imaging can provide images: in real-time; at clinically relevant depths; with relatively high spatial

[*]**Corresponding author**: Sanjiv S. Gambhir, MD, PhD; Chair, Department of Radiology, Director, Molecular Imaging Program at Stanford (MIPS); Professor, Department of Radiology, Department of Bioengineering, and Department of Materials Science & Engineering. Member, Bio-X Program; The James H Clark Center, 318 Campus Drive, East Wing, 1st Floor, Stanford, CA 94305-5427 Ph: 650-725-2309; Fax: 650-724-4948; sgambhir@stanford.edu.

The authors disclose no potential conflicts of interest.

resolution; and without the use of ionizing radiation. Photoacoustic imaging can be performed either by (1) relying on intrinsic tissue contrast alone (e.g., mapping endogenous chromophores such as melanin, hemoglobin, and lipids); or by (2) using exogenous molecular imaging agents that can either target specific molecular processes (targeted agents) or extravasate due to leaky vasculature and the enhanced permeability and retention (EPR) effect found in tumor tissue (non-targeted agents).

In this review we will first describe the basics of photoacoustic imaging, followed by a comprehensive overview of its clinical applications. We will then discuss strategies for future translation to clinical practice.

Principles of photoacoustic imaging

Photoacoustic imaging relies on the photoacoustic effect, first described by Alexander Graham Bell (1). In short, a pulsed nanosecond-long red-shifted laser beam is used to illuminate the tissue(s) of interest causing photons to propagate diffusely inside. The absorption of these photons leads to a slight localized heating of the tissue causing thermoelastic expansion. This transient thermoelastic tissue expansion generates pressure waves (ultrasound), which can then be detected by broadband ultrasonic transducers, and converted into images. These basic principles are illustrated in a potential clinical application (see Figure 1). The shared detector platform (the detector array) facilitates a natural integration of PAI and ultrasound imaging (US) creating a hybrid imaging technique that combines functional (PAI) and structural (US) information, which is favorable for clinical translation (Figure 1). Additionally, the fact that photoacoustic imaging is similar to US in technology and handling - it can also itself be real-time, portable, relatively cheap, and safe (non-ionizing radiation) - makes it even more adoptable/integrable for clinicians.

The combined use of light and sound in PAI has an important advantage over other imaging techniques such as optical imaging, US, magnetic resonance imaging (MRI), computed tomography (CT), positron emission tomography (PET), and single-photon emission computed tomography (SPECT), namely the unique scalability of its spatial resolution and depth penetration across both optical and ultrasonic dimensions. In optical imaging, scattering of light hinders penetration depth, while in PAI the detection of acoustic signal, which has much lower tissue scattering, allows for superior depth penetration. Spatial resolution can be very high (microscopic level) at higher ultrasound frequencies, but with lower depth penetration, as a trade-off, due to the increasing attenuation of ultrasound with frequency. Photoacoustic microscopy (PAM) generates lateral resolutions down to 45 μm at a depth of 3 mm when using ultrasound frequencies of 50 MHz (2-5), and this can even improve to 200 nm (subcellular level) in optical-resolution PAM, but only at imaging depths of up to 1 mm (6). Macroscopic PAI systems allow for deeper tissue imaging by using lower ultrasound frequencies of 4-8 MHz and typically generate resolutions of 0.5-5 mm at reported imaging depths of ~3-7 cm (3, 6-10). A summary of the largest depths reached with macroscopic PAI systems is presented in Table 1. The unique scalability of spatial resolution and imaging depth may afford a wide breadth of imaging ranging from the microscopic to the macroscopic scale, something that is very challenging to do utilizing most other imaging modalities. For example, comparing optical microscopy images to computed tomography images is difficult because the image contrast is obtained in entirely different ways (optical absorption vs. x-rays). Thus PAI could open up inimitable opportunities to study complex biological systems and pathways in the same organism from the subcellular level to the organ level, using the same optical absorption contrast. Some PAI systems can already image both at the macroscopic and microscopic level (11), although so far most systems have been designed to image specifically at one or the other of these levels. Although spatial resolution of PAI may be superior over other imaging

techniques such as PET and SPECT (12), we have to keep in mind that these modalities do not suffer from depth limitations (as attenuation of gamma rays can be corrected for) which makes them suitable for whole body imaging. Most likely PAI will be used in adjunct to clinically established imaging techniques, or in combination with them in a multi-modality setting. More information on these multi-modality imaging approaches in which anatomical and molecular information are combined, can be found under the organ specific sections of this review.

Another key advantage of PAI, mentioned earlier, is that the optical component of the technique allows for molecular imaging even without the use of an imaging agent, by utilizing multiple wavelengths (multispectral imaging of endogenous contrast). Different tissue components have unique optical scattering and absorption properties for each wavelength. In Figure 2 the absorption spectra for the main light absorbing tissue components (oxy- and deoxyhemoglobin, lipid, water, and melanin) are shown. As seen from this figure, total light absorbance in these tissue components is lowest in the wavelength range of 600-1000 nm, referred to as the near-infrared (NIR) or “optical window”. Since the absorbance is lowest in the NIR range, light of these wavelengths is used to obtain sufficient tissue penetration depth (a few centimeters). Information on tissue composition, i.e., relative concentrations of (de)oxyhemoglobin, water, lipid, or an injected imaging agent, can be calculated by combining photoacoustic data acquired at multiple wavelengths. Numerous relevant clinical parameters can be assessed this way, for example hypoxia, perfusion, and neoangiogenesis.

Many different PAI-platforms for clinical use already exist or are under development including handheld probes and PA computed tomography (PAT) as exemplified under the organ specific sections that follow. In short, PAI systems can be categorized as linear array systems (13-16) or tomographic systems (9, 17). Tomographic systems detect photoacoustic waves emanating from the ‘entire’ perimeter of the subject of interest using either a single element or an array transducer. In linear array systems, an ultrasound array is used to detect photoacoustic waves from ‘limited angles’ around the object. The limited field of view results in an image quality inferior to that of tomographic systems. However, linear array systems are more portable and can be integrated into already existing clinical ultrasound systems, enabling the visualization of organs less accessible with tomographic systems (e.g., via endoscopes or catheters).

During the last few decades major progress has been made in source and detector development, allowing for instance for faster (real-time) imaging at more wavelengths and greater depth penetration (18). Light propagation models and image reconstruction algorithms have improved significantly also (18-23), which is critical to image quantitation. Obtaining truly quantitative images is only possible when correcting for the amount of light delivered to an actual tissue depth, and this remains challenging because light attenuation depends on several factors, not only the imaging depth but also the tissue type in which the light propagates.

The abovementioned progress in technology plus the inherent advantages of photoacoustic imaging are paving the way for clinical translation of the technique. A summary of potential clinical applications of photoacoustic imaging in different organ systems is illustrated in Figure 3. More detailed descriptions of the principles of photoacoustics can be found in book chapters (24, 25) and other papers covering this topic (17, 26-28).

Imaging contrast

Endogenous contrast

Photoacoustic imaging takes advantage of the fact that the body tissues contain a variety of endogenous chromophores with different absorption spectra, such as melanin, water, fat, $Hb0_2$ (oxyhemoglobin) and Hb (deoxyhemoglobin), as shown in Figure 2. Many diseases cause changes in tissue composition, such as neovasculature in cancer development (29) and vascular fat deposition in atherosclerotic plaques (30). PAI has the potential to visualize and quantify these changes in comparison to the normal surrounding tissue. PAI based on endogenous contrast alone has been studied for various diseases (e.g., atherosclerosis, breast cancer, and prostate cancer) (30-32). However, not all absorption spectra for different tissues are known. Multi-wavelength PAI makes it possible to image several tissue components in the same image, although the need for a tunable pulsed laser source increases the costs of the system significantly. Because some tissue components have very similar absorption spectra within the NIR range, there is sometimes a need for exogenous molecular imaging agents to enhance the contrast. Moreover, exogenous imaging agents can potentially facilitate deeper tissue imaging.

Exogenous imaging agents

Exogenous imaging agents can greatly enhance the photoacoustic imaging contrast. One could use non-targeted imaging agents that mostly extravasate from the blood stream due to increased vascular permeability and the EPR effect in tumorous tissue, or targeted imaging agents that target a specific molecular process, i.e., a certain receptor, protein, or enzyme. The advantage of targeted imaging agents is that they can provide specific information on molecular or cellular processes in the tissue. There is a great variety of imaging agents that can be used for photoacoustic imaging (see Table 2, Figure 4). The selection of a particular imaging agent will depend upon the application for which it will be used and one should thoroughly consider various characteristics, such as the size, shape, toxicity, stability, surface chemistry, and targeting moieties of the imaging agent. Besides a few imaging dyes that have been approved for human use (Indocyanine Green; ICG, Evans blue; EB, and methylene blue; MB), the rest of the imaging agents are not yet approved, and have only been evaluated in phantoms or animal models. Thus far, not much information is available on the mass range that is needed for any of the potential imaging agents to perform their respective photoacoustic imaging studies. This is an important issue and the toxicity of these imaging agents will have to be determined relative to the mass needed to be injected in order to perform a given study. It is likely that higher masses will be necessary for photoacoustic imaging studies compared to very sensitive techniques such as PET and SPECT. Mass ranges will have to be assessed for each specific agent and its applications.

Small molecule dyes—There is a range of small molecule dyes that absorb in the NIR window and can thus be used for PAI. Many of these dyes are fluorescent and are commonly used in optical fluorescence imaging. The difference with PAI is that for this technique only the absorption part of the spectrum is utilized and not the fluorescent emission part, making it more efficient to have a low quantum yield (i.e. a low ratio of photons emitted to photons absorbed, since more of the absorbed energy can be converted into PA signal). The dyes can be used as agents that are not targeted, but can also be functionalized to enable molecular targeting. For example a dye can be directly conjugated to a targeting antibody such as trastuzumab to image Her2 expression (33) or to a caspase-binder to image apoptosis (34). Furthermore, an activatable probe has been designed by our laboratory especially for photoacoustic imaging, using activatable cell-penetrating peptide as its peptide platform with a NIR chromophore (quencher or fluorophore) on either side of this platform to enable dual-wavelength imaging. The intact probe is photoacoustically silent through subtraction of

the images obtained at the two wavelengths, but after activation by matrix metalloproteinases (MMPs), specifically MMP-2, the cleaved probe shows a change in photoacoustic signal because now only the cell-penetrating peptide portion of the probe (carrying one of the chromophores) accumulates in the cells and the rest of the probe (carrying the other chromophore) diffuses away (35). This platform is generalizable and can be tailored to the target proteases of interest, but its potential was recently shown in mice *in vivo* for photoacoustic imaging of thyroid carcinoma (36). Additionally, Razansky et al. showed that the commercially available activatable fluorescent probe MMPSense 680 can be used for molecular imaging with photoacoustic imaging systems as well (37). MMPSense 680 also undergoes changes in light absorption after activation by MMPs. These changes can then be spectrally resolved over the inactivated probe and the background by acquiring the photoacoustic signal over a range of wavelengths, compared to the two-wavelength imaging used for the previously described activatable photoacoustic probe.

The advantages of the small molecule dyes (~ 1 nm in size) are their biocompatibility and their fast and complete clearance from the body due to their small size. This makes them valid candidates for clinical use. As mentioned earlier, a few biocompatible dyes have already been approved for clinical use (ICG, EB, and MB). These dyes have been studied in various animal models for PAI (3, 38-43), but not yet in clinical trials. The downside of their small size is that it is less likely for the imaging agents to be delivered to or retained at the target site during their short circulation time. In addition, photostability is an important issue for these dyes since they suffer from photobleaching (loss of optical absorption) after exposure to prolonged laser irradiation. Circulation time and photostability can be improved by encapsulating more dye molecules into a bigger nanoparticle, which was shown by Kim and colleagues who developed ICG-embedded nanoparticles based on PEBBLE (photonic explorers for biomedical use by biologically localized embedding) technology (44). In PEBBLE, high dye concentrations are encapsulated into biocompatible nanoparticles, for example, an ormosil matrix was used by Kim et al. for nanoparticle synthesis and each particle was loaded with > 20,000 ICG molecules. Gupta et al. also encapsulated many ICG molecules into bigger nanoparticles, but they made a construct comprised of a protein shell, purified from the plant-infecting brome mosaic virus (BMV), to encapsulate the ICG (45).

Nanoparticles—Nanoparticles are larger in size than small molecules. Their size varies between a few to several hundred nm. Based on their mechanism, the nanoparticles can be divided into two categories: plasmonic and nonplasmonic nanoparticles. The plasmonic nanoparticles are made of a noble metal (gold, silver) and utilize the surface plasmon resonance effect (SPR). This effect takes place when the electromagnetic field of incoming light interacts with the conduction electrons on the surface of the nanoparticle, resulting in mutual oscillation of these electrons at a resonance frequency relative to the lattice of positive ions. At this resonance frequency, the incoming light is absorbed by the nanoparticle, with an optical absorption that is five orders of magnitude greater than the absorption for dyes (on a per particle basis) (25).

The plasmonic nanoparticles exist in numerous sizes and shapes (see Table 2). The most commonly used kinds in PAI are nanoshells, nanorods, and nanocages, usually made of gold (46-57). Besides these regular shapes, some more complex shapes have been designed, such as nanostars, nanoroses, nanowontons, and nanoclusters (58-62)(52-56). The advantage of these plasmonic nanoparticles is that their optical properties (absorption and scattering) are highly tunable over the NIR spectrum by changing their size or shape, which makes them very attractive for biomedical applications. An additional important advantage is that the surface characteristics of these nanoparticles are easy to chemically modify, which is important for *in vivo* use (e.g., to decrease cytotoxicity or to increase circulation time and stability) and for molecular targeting. Functional groups such as polyethylene glycol (PEG)

or integrins can be attached to the surface in a straightforward way. The disadvantages of plasmonic nanoparticles are that they can deform after extended exposure to laser irradiation and that their long-term safety is a concern, especially with the larger particles that do not fully clear the body as they are taken up by the reticuloendothelial system (RES). The deformation of nanoparticles affects the photoacoustic signal and results in inconsistent imaging results over time. A thin layer of silica coating can increase stability of the nanoparticles and allow them to maintain their original shape for a longer time (63). An extra advantage of the silica coating is that these hybrid nanoparticles can act as photoacoustic nanoamplifiers due to more efficient heat dissipation to the tissue (64). Zhang et al. have demonstrated a new type of nanoparticle for photoacoustic imaging. In addition to using conjugates of fluorescent nanodiamonds and gold nanoparticles to enhance their otherwise low photoacoustic signal (65), they have shown the feasibility of utilizing nanodiamonds damaged by helium ion irradiation (66). These radiation-damaged nanoparticles gave a 70-fold higher photoacoustic signal compared to gold nanoparticles of similar dimensions, caused by increased optical absorption due to vacancies in the diamond crystal lattice.

The nonplasmonic nanoparticles are strong light absorbers that do not rely on the SPR effect. Single-walled carbon nanotubes (SWNTs) are the most widely used example of nonplasmonic nanoparticles. They absorb light over a broad spectrum, including the NIR range. Their broad absorption spectrum even allows for “thermoacoustic imaging” using lower energy electromagnetic waves (microwaves instead of NIR light) (67). Like the plasmonic nanoparticles, the nonplasmonic nanoparticles can also be modified to improve their functionality. For example, several dyes can be attached to the SWNTs to increase light absorption and targeting agents can be conjugated to the SWNTs for molecular imaging purposes (Figure 4) (68-70). In addition, the SWNTs can be coated with a thin layer of gold, which enhances the photoacoustic signal since with this layering the SPR effect is utilized (71). Another type of nonplasmonic nanoparticle is a structure in which several dye molecules are grouped together, with stronger light absorption and longer circulation time than for the free dye. For example, the ICG-embedded PEBBLEs by Kim et al. are ormosil spheres containing many ICG dye molecules, and it was shown that Her2-antibodies could be attached to the surface of these nanoparticles for cancer targeting (44). Quantum dots are semiconductor nanoparticles that are strongly fluorescent with sizes ranging from 2-10 nm. Shashkov et al. showed in their studies that these quantum dots can also be used as photoacoustic imaging agents (72). Copper sulfide nanoparticles, ~11 nm in diameter, also have these semiconductor characteristics and produce photoacoustic signal at longer wavelengths (1064 nm) as shown by Ku et al. (73).

Limitations of SWNTs for human clinical applications comprise mainly the (long-term) toxicity concerns (74). Although the first systematic toxicity evaluation of functionalized SWNTs following intravenous injection in living mice did not show signs of acute or chronic toxicity, more evidence is needed to determine the safety of these SWNTs for *in vivo* medical applications (75). The nanoparticles encapsulating dyes have the problem of photobleaching, however, their stability can increase up to 500% compared to the free dye (76). Additionally, the surface of the encapsulated dyes can potentially be easier to chemically modify than just the free dye by itself. Quantum dots are highly photostable, but their main drawback for biomedical applications is that their major components, cadmium and selenium, are toxic to cells and organisms (77).

Depending on their characteristics, the nanoparticles can also be loaded with drugs and used as delivery vehicles to allow for simultaneous delivery of therapeutic and imaging agents in vivo (78, 79), or their intrinsic properties can be utilized for photothermal ablation therapy

(80). This provides great opportunities for image-guided therapy / theranostics (combining therapy and diagnostics).

Multimodality imaging agents—Since imaging is becoming increasingly important in the diagnosis and treatment of disease, imaging agents that can be tracked by multiple imaging modalities can be very useful in overcoming the limitations of a single imaging modality in the different steps of the diagnosis/treatment process (e.g., using different modalities for whole body diagnostic imaging before surgery versus real-time intraoperative imaging). Multimodality imaging agents that can enhance contrast for PAI in combination with other imaging modalities are under development. Nanoparticles that are both plasmonic and superparamagnetic can be used for combined photoacoustic and magnetic resonance imaging (MRI); examples are nanostars, nanoroses, pearl necklaces, nanowontons, iron oxide and gold-coupled core–shell nanoparticles, and liposomes containing iron oxide nanospheres and gold nanorods (58-62, 80-82). Kim et al. used multifunctional microbubbles and nanobubbles for concurrent photoacoustic and ultrasound imaging in phantoms (83). Wilson et al. developed photoacoustic nanodroplets, consisting of a droplet of liquid phase shift perfluorocarbon with a bovine serum albumin shell in which optically absorbing nanoparticles have been suspended (84). These nanodroplets act as dual-imaging agents for both photoacoustic and ultrasound imaging through optically triggered vaporization. Gold nanorods have been labeled by ^{125}-I to allow for dual-mode SPECT and PAI after intra-articular injection in rat tails (85). For a triple-modality approach of *M*agnetic resonance imaging, *P*hotoacoustic imaging, and *R*aman imaging, our research group recently developed ‘MPR’ nanoparticles by modifying gold-based Surface Enhanced Raman Scattering (SERS) nanoparticles with Gadolinium (86). This novel molecular imaging agent was then used to accurately help delineate the margins of brain tumors in living mice (Figure 5). Recently, Grootendorst and colleagues proposed to use a commercially available MRI agent (Endorem; superparamagnetic iron oxide nanoparticles), as a photoacoustic probe for intraoperative imaging of lymph nodes and demonstrated the feasibility *ex vivo* in rats (87).

Genetically encoded probes—Genetically encoded fluorescent proteins have been widely used for more than a decade in preclinical optical imaging studies. The use of photoacoustic imaging for reporter gene imaging was first demonstrated by the Wang group in 2007 (88). They used the lacZ gene, which encodes the enzyme β-galactosidase. After injection of a colorless analogue of lactose, ‘X-gal’, cleavage of this substrate by β-galactosidase eventually leads to formation of a blue product, which can then be detected by photoacoustic imaging due to its high optical absorption. In later studies they showed that they could reach imaging depths of ~5 cm with this technique, with spatial resolutions of ~1 mm, which is a major improvement over traditional optical (bioluminescence or fluorescence) reporter gene imaging, reaching depths of up to ~1 cm (89). Filonov et al. showed that a bacteriophytochrome-based near-infrared fluorescent protein named iRFP could also serve as a probe for PAI (90). It can produce stronger photoacoustic signal than blood in the NIR window, does not require injection of exogenous substrates, and can be delivered into the body by standard genetic manipulations of cells. Ha and colleagues then reported the potential of ferritin as a reporter gene suitable for photoacoustic imaging *in vitro* (91). Recently, Qin and colleagues demonstrated *in vitro* and *in vivo* in mice that the tyrosinase gene as a single reporter gene could be used for triple modality imaging by PAI, MRI, and PET, through catalyzing the synthesis of melanin (92). These genetically encoded proteins have vast potential for whole body animal imaging, however, the use of genetically encoded probes remains challenging for human applications due to the requirement of introduction of a reporter gene. Nevertheless, for many small animal model applications or cell therapy applications in humans, reporter gene strategies provide a potentially powerful approach.

Clinical Applications

Breast imaging

The conventional techniques for breast imaging include digital mammography (DM), ultrasonography (US), scintimammography, and MRI. A combination of these methods usually yields relatively high sensitivity and specificity for cancer detection. Each of the techniques has some drawbacks. Mammography is associated with ionizing radiation and has decreased sensitivity for cancer detection in dense breasts. The results of US greatly depend on the instrument performance and examiner's skill. MRI requires more time and cost and requires the use of imaging agents, to get dynamic information about neovascularization. New imaging technologies are needed that can aid in early detection of breast cancer and provide comprehensive information of the tumor properties potentially important for treatment decision and especially in assessment of response to therapy. Increased use of preoperative systemic therapy and differentiation of therapy in general, depending on the tumor properties, require more functional/molecular tumor information that PAI may be able to provide.

PAI is now being investigated in initial patient studies in breast imaging. Five studies published so far have involved patients (8, 9, 31, 93, 94). Two of the studies are continuing clinical attempts with the The Twente Photoacoustic Mammascope (PAM), developed at the University of Twente in the Netherlands. It consists of a bed on which the patient lies in the prone position with her breast pendant through an aperture. In the scanning compartment of the system, the breast is gently compressed between a glass plate and a flat ultrasound detector matrix, with acoustic coupling gel applied between the breast and the detector. The system was first tested and evaluated in breast tissue phantoms (95, 96) and in 2007 two out of five clinical breast cancer cases were presented (8). In 2012, this group then presented 10 cases of breast malignancy and two cases of benign cysts (94). PAM imaging revealed higher intensity regions based on increased optical absorption that could be attributed to the cancer-associated vascular distribution. This increased photoacoustic contrast was absent in the cysts. However, the PA contrast seemed to be independent of the mammographically estimated breast density, a promising observation for imaging patients with dense breast tissue (currently limited by decreased mammographic sensitivity). In these studies, 13 of 30 (first 8 of 13 and then 5 of 17) measurements could not be included in the analysis due to technical reasons. These technical issues, such as the inability to image lesions located close to the chest wall, are challenging in the design of improved photoacoustic breast imaging systems. An example of a breast cancer imaged with mammography, US, and PAI is shown in Figure 6.

Ermilov and colleagues investigated a laser-based optoacoustic system (LOIS) with a 64-element-annular array of rectangular transducer elements surrounding a hemicylindrical volume in which the breast was suspended (31). A pulsed laser operating at 755 nm illuminated the breast and single planes through the breast were captured one at a time. The spatial resolution was reported to be 0.5 mm. Preliminary clinical studies on 27 patients with suspicious breast lesions on mammogram and/or ultrasound were presented. The LOIS-64 was able to visualize 18 out of 20 malignant lesions, as was confirmed by breast biopsy performed after the photoacoustic imaging procedure.

Kruger and colleagues recently modified a small animal photoacoustic tomography (PAT) system to image human breasts (9). Two 3D maximum intensity point (MIP) projections of the left breast of a healthy volunteer were generated, depicting sub-millimeter vessels to a depth of 40 mm without the use of a molecular imaging agent (see supplementary file, http://www.optosonics.com/breast-images.html). So far no breast cancer patients have been

imaged with this system, but neoplastic breast lesions could potentially be visualized based on their hemoglobin content.

Kitai et al. recently published a paper in which 27 tumors in 26 subjects were visualized using a prototype photoacoustic mammography system (93). The patients were examined lying in the prone position with the breasts mildly compressed in a craniocaudal direction between holding plates. Pulsed laser beams irradiated the breast from both sides, and photoacoustic signals were detected on the caudal side by a transducer array. The measurable area was 30 mm × 46 mm for one scan, which took 45 s. The lesions included 21 invasive breast cancers (IBC), five ductal carcinoma in situ (DCIS), and one phyllodes tumor. Nine out of twenty-one IBC patients had received primary systemic therapy (PST). Eight out of twelve IBC without PST were visible.

Detection was possible in all five cases with DCIS, whereas it was not in the one case with phyllodes tumor. Seven out of nine IBC with PST were assigned as visible in spite of decreased tumor size after PST. The mean value of hemoglobin saturation in the blood vessels of visible lesions was 78.6 % (they reported values of > 92% for normal subcutaneous blood vessels) and the average total hemoglobin content in these lesions was 207 μ M. These encouraging results show the potential to evaluate and quantify functional information, which may be useful in diagnosing and assessing treatment response in breast cancer.

Other systems with potential applications for breast cancer imaging have been developed, but not yet clinically tested. The optoacoustic plus ultrasound system (OPUS), is a handheld combination of a wavelength-tunable pulsed laser and a commercial ultrasound scanner (97). By employing suitable image reconstruction algorithms and quantification procedures, a linear relation between local optical absorption and PA signal was found for absorbers at different depths and optical matrix properties.

The Wang laboratory has developed an integrated photoacoustic tomography and thermoacoustic tomography (PAT/TAT) system that combines nonionizing radiofrequency waves and NIR laser light to obtain additional information from breast tissue, such as water/ion concentration, blood volume, and oxygenation level of hemoglobin (98). As opposed to breast compression from the sides, used in x-ray mammography, this PAT/TAT scanner uses front compression to give the breast a cylindrical shape and obtain a full 3D data set. The front compression may possibly allow for imaging the regions close to the chest wall. Also, dry coupling is used instead of the usual coupling gel in conventional ultrasound imaging. Good quality PAT and TAT images on tissue mimicking phantoms have so far been achieved (98, 99).

So far, out of all of the potential clinical applications, translation of photoacoustic imaging has reached the furthest in breast imaging. Several groups are working on improved clinical systems with better depth penetration and higher spatial resolution (100, 101), which will help move photoacoustic breast imaging forward.

Sentinel lymph node detection in breast cancer—The presence of axillary lymph node metastases is the most important factor in staging of early breast cancer and during the last decade, sentinel lymph node biopsy (SLNB) has taken a leading role in the staging procedure. Although SLNB could also be useful in other type of cancers, for example melanoma or Merkel cell carcinoma (an aggressive form of skin cancer), it is most widely used in breast cancer and we will therefore focus on this application. Sentinel lymph nodes (SLN) are defined as the first lymph nodes (usually a cluster of 3-4 nodes) in a tumor bed that receive lymphatic drainage from the tumor tissues. These nodes are thus most likely to

harbor any metastasizing cancer cells along the path of lymph drainage of tumor tissues (102). The SLNB technique usually involves injection at the breast tumor site with the combination of a radiolabeled sulfur colloid and a blue dye. The clinical procedure varies, but can involve pre-surgical scintigraphic imaging, and pre/peri- operative use of a gamma probe or Geiger counter to locate the SLN. After visual confirmation the SLN is surgically resected, and the definitive presence of cancer is established with histological methods. SLNB can help avoiding morbidities associated with complete axillary nodal dissection, which was the prior standard. So far, radiocolloids and blue dyes are generally considered complementary in SLNB and should both be used routinely. However, the procedure could be done without involving radioactivity if the signal from the blue dye alone could be detected in real-time pre/peri-operatively with PAI and in combination with ultrasound for anatomical information. Although to a lesser extent, morbidity has also been reported after SLNB (103, 104). Possibly a PAI guided approach could avoid surgical intervention of the sentinel node and instead guide a fine-needle aspiration. If PAI allows for noninvasive identification of the SLN, the combination of fine-needle aspiration biopsy and real-time reverse transcription-polymerase chain reaction to confirm lymph node status (malignant/benign) might be a minimally invasive alternative to SLNB.

Using photoacoustic imaging, Song et al. accurately mapped SLNs noninvasively in living mice and rats upon injection of Evans blue, a blue dye currently used in clinical SLNB (41). They were also able to mimic photoacoustic imaging of ‘deeper’ SLNs by layering additional biological tissues on top of the rats (>3 cm) and injecting either methylene blue (40), indocyanine green (38), or gold nanocages (105). ICG stained SNL PA imaging is shown in Figure 7. In addition, the Wang group has reported *in vivo* PA and US mapping of ICG or methylene blue stained SLNs in rats using a clinical US array system, and they also demonstrated guidance of SLN fine needle aspiration biopsies using this technique (7, 106, 107). SNL detection by PAI and ICG-enhanced SWNTs was evaluated in rats by Koo et al. (70). Akers et al. recently reported the use of SPECT/CT to validate PAT in SLN detection (108). While SLN imaging is a PAI application under intensive research in animal models *in vivo*, its feasibility remains to be shown in humans.

Urologic imaging

Prostate imaging—Standard screening and diagnostic methods for prostate cancer - such as blood screening for prostate specific antigen (PSA) and other biomarkers, digital rectal examination (DRE), and transrectal ultrasound (TRUS) guided prostate biopsy – have limited ability (sensitivity and specificity) in the early diagnosis of prostate cancer (109, 110). Furthermore, the available techniques cannot fully differentiate between aggressive and more latent prostate cancers with the consequence that there is no significant impact on survival. This leads to overdiagnosis and overtreatment (110). A combined transrectal probe with US and PAI for prostate imaging to combine anatomical, functional and molecular imaging is a potentially useful approach to move prostate imaging and diagnosis forward. To date, there are no reports on PAI for prostate imaging in humans, yet several groups have conducted promising studies *in vivo*. In canine prostates induced blood lesions have successfully been imaged (111-113) (Figure 8), in a rat model prostate adenocarcinoma tumors have been visualized (32), and in a mouse window chamber model prostate tumor progression has been imaged with 3D photoacoustic and pulse echo imaging, both without the use of a molecular imaging agent (114), and with the use of gold nanorods to enhance image contrast (115). ICG embedded PEBBLEs (photonic explorers for biomedical use by biologically localized embedding-defined on p.10) conjugated with HER-2 antibody showed high contrast and high efficiency for binding to prostate cancer cells in initial *in vitro* characterization studies (44).

Among the treatment options available for prostate cancer, the use of brachytherapy seeds, metal implants that deliver localized radiation therapy, is an important clinical approach (116, 117). Since visualization of the small seeds can be difficult, the TRUS-derived position of the needles delivering the seeds to the tissues is often relied upon to infer seed placement. Correct seed placement is important for dose planning management. Because metals have an optical absorption that is orders of magnitude greater than that of soft tissue, PAI may be very valuable as an adjunct to TRUS in seed placement imaging. Su and colleagues experimentally evaluated PAI in combination with TRUS for brachytherapy seed visualization in excised bovine prostate tissue. They found that PAI improved imaging contrast with 2.7 to 27.9 dB over TRUS alone (for seeds in the long-axis orientation) at imaging depths ranging from 4 to 13 mm (118). Harrison and Zemp investigated PAI for brachytherapy seed visualization in a tissue phantom, comparing the received intensity to endogenous contrast. They found that PAI at 1064 nm could identify brachytherapy seeds uniquely at laser penetration depths of 5 cm in biological tissue at the ANSI limit for human exposure with a contrast-to-noise ratio of 26.5 dB (119). Kuo et al. recently showed imaging of brachytherapy seeds in an *ex-vivo* dog prostate phantom (120).

In summary, to move the clinical translation of photoacoustic prostate imaging forward there is a need for the development of a transrectal PAI/US device with sufficient depth penetration and spatial resolution. Also, better characterization of biological prostate tumor signatures (e.g., cell surface receptors, degree of vascularization) is important to identify potential targets for a more specific diagnosis of prostate cancer by PAI, with or without the use of extrinsic molecular imaging agents.

Bladder imaging—Since urethrocystoscopy cannot determine the extent of invasive bladder cancer and is not always able to discriminate between flat carcinoma in situ and inflammation, photoacoustic imaging may be able to give additional diagnostic and/or prognostic information in these cases. In an initial study by Xie and colleagues, the bladder microvasculature was successfully visualized *ex vivo* using microscopic PAI on canine and human bladder specimens (98).

A different application is evaluation of vesicoureteral reflux (VUR). VUR is abnormal leakage of urine from the bladder to the upper urinary tract, which may be a source of infections and eventually renal scarring, especially in children. Current imaging methods to diagnose and monitor VUR are x-ray or radionuclide based and the possibility to use US/PAI instead, and hence avoid ionizing radiation in children, would be a step forward. Kim et al. explored noninvasive photoacoustic bladder imaging *in vivo* by mapping rat bladders filled with methylene blue (121, 122), whereas Koo et al. visualized the rat bladders using ICG-enhanced SWNTs (70). These methods may in the future be useful for vesicoureteral reflux (VUR) monitoring in children.

Photoacoustic bladder imaging is certainly in its infancy and many technical issues need to be resolved before clinical translation is feasible. Additionally, further investigations of exogenous molecular imaging agents, especially regarding safety and suitability for this application, are warranted before exploration of the technique in humans.

Dermatologic imaging

Melanoma is the most aggressive form of cutaneous cancer, and the most difficult to diagnose and stage (123). Detection typically relies on visual evaluation of the morphology of a lesion, followed by biopsy and histopathologic assessment of suspicious lesions. To improve melanoma detection, various noninvasive imaging techniques, including photoacoustic imaging, are under investigation. Most melanomas contain melanin, which is a highly light absorbing pigment. Melanin provides great contrast for photoacoustic imaging

in the “optical window” (~600-1000 nm, see Figure 2) without having to inject an imaging agent. Photoacoustic microscopy (PAM) is most frequently explored for melanoma detection and staging, using various imaging systems such as dark-field PAM, with depth penetrations of up to 3 mm (17). The first proof of principle of this technique *in vivo* was shown by Zhang et al., imaging angiogenesis, melanoma, and SO_2 of single vessels in animals, and total hemoglobin concentration in humans (2). This group illustrated that dual-wavelength imaging can separate the contributions from two different pigments, in this case hemoglobin and melanin, based on their absorption spectra. In further studies they measured the metabolic rate of oxygen in melanoma using PAM (124). Additionally, they demonstrated that targeted melanoma imaging could enhance the photoacoustic contrast by ~300%, utilizing bioconjugated gold nanocages targeted to the α-melanocyte-stimulating hormone receptors over-expressed on melanomas (Figure 9) (53). Favazza and colleagues investigated PAM *in vivo* in volunteers by imaging a melanocytic nevus and assessing the vascular and structural differences between palm and forearm skin (125). Recently, photoacoustic detection of melanoma metastases based on their melanin content proved to be possible in resected human lymph nodes (126). In summary, PAM can noninvasively (without the use of an imaging agent) obtain functional information on tissue that may be helpful in the diagnosis and staging of melanoma. Biopsy is the standard method for histology and diagnosis of melanoma, although it relies on biopsying a representative area of the often heterogeneous tumor. With the use of PAM, it might be possible to “map” the lesion and guide what area to biopsy, potentially increasing the diagnostic accuracy and avoiding unnecessary biopsies. One of the challenges is that a subgroup of melanomas does not contain melanin, and thus require a different photoacoustic imaging approach, possibly involving the injection of a molecular imaging agent. Another critical point in the development of more accurate diagnostic tools is the need for a high resolution technique to decide if the cancer cells have invaded through the basement membrane (123), enabling them to spread to distant tissues. Further *in vivo* studies are thus required to determine whether PAM can meet these clinical needs.

In addition to assessing malignant melanoma, photoacoustic imaging may also be valuable in the evaluation of other skin conditions, such as burn wounds. Since clinical characterization of burn wounds can be challenging, the assessment of tissue viability by imaging intact dermal vasculature may help in determining an appropriate treatment plan. So far, PAM has been explored for burn wound assessment in rat and pig models with promising results (127-130). Human studies have not been performed yet, but this seems to be within reach in the near future.

Gynecologic imaging

Ovarian cancer has the highest mortality of all gynecologic cancers due to late onset of symptoms in combination with a lack of effective methods for early detection (58). At present, there is no existing evidence that any screening test, including CA-125, US, or pelvic examination, reduces mortality from ovarian cancer (131). The currently used imaging techniques, for instance US, have poor sensitivity and specificity for the detection of early-stage cancers (132). Since PAI can be easily integrated in a clinical US system, such a dual system could potentially enhance the diagnostic accuracy of ovarian cancer detection. Aguirre et al. developed a noninvasive transvaginal co-registered 3D ultrasound and PAI-system, and evaluated the optical properties of normal porcine ovarian tissue with this system in vivo (133). The results showed strong light absorption from highly vascularized corpora lutea and low absorption from follicles, demonstrating that PAI is capable of detecting vascularized structures in the ovaries, otherwise not visible with ultrasound. These findings were further evaluated in 33 *ex vivo* human ovaries (134). Quantification of the light absorption levels in the ovary indicated that, in the postmenopausal group, malignant

ovaries showed significantly higher light absorption than normal ones (P = 0.0237) corresponding to a sensitivity of 83% and a specificity of 83%. The same group presented an integrated optical coherence tomography (OCT), ultrasound (US), and photoacoustic imaging (PAI) prototype endoscopy system, with a diameter suitable for insertion through a standard endoscopic laparoscopic port during minimally invasive surgery (5 mm) (135). Porcine and human ovarian tissues were imaged successfully *ex vivo*, showing the potential of the hybrid device over each modality alone in ovarian tissue characterization. Kumavor et al. have recently developed a co-registered pulse-echo/photoacoustic transvaginal probe and in initial experiments human ovaries *ex vivo* were imaged (136). The mentioned combined techniques for ovarian imaging show promise for clinical translation, but results remain to be validated *in vivo and* eventually tested for diagnostic accuracy compared to existing imaging techniques. PAI could potentially also play a role in other gynecological diseases, such as cervical and endometrial cancer, but thus far these areas have not been explored.

Hematologic imaging

Circulating tumor cells (CTCs) can often be detected in the blood of patients with early or advanced cancer by antibody-based assays or molecular methods. CTC detection is an area of intense research, studying patients with different types of cancer, including breast, colorectal, prostate, and skin cancer. In several studies, CTC detection in early and/or metastatic disease has been shown to correlate with unfavorable clinical outcome (137). There are several different technologies for CTC detection *ex vivo*, but the two main approaches are the use of monoclonal antibodies directed against histogenic proteins (e.g., cytokeratins, CK and epithelial cell adhesion molecule, EpCAM) and PCR-based molecular assays amplifying tissue-specific transcripts (138). The major drawback for both of these techniques is their limited sensitivity due to the analysis of only small blood volumes. To overcome this problem, flow cytometry techniques could be utilized to assess larger blood volumes *in vivo*. The fluorescent labels commonly used in flow cytometry have certain limitations, such as their potential toxicity and immune response to the fluorescent tags. Photoacoustic flow cytometry has the advantage that label-free detection of cells with high absorption/scattering characteristics, such as the CTCs from melanomas for instance, is possible. Malignant melanomas are known to metastasize at early stages and the presence of CTCs appears to be a prognostic marker (139, 140). The intrinsic photoacoustic contrast coming from the melanin in the cells, makes photoacoustic flow cytometry an ideal candidate for the label-free detection of CTCs from melanoma, as has been shown by several research groups *in vivo* (141-145) as well as *in vivo* (146-148). Nedosekin et al. recently reported on *in vivo* ultra-fast PA flow cytometry, showing the detection of circulating human melanoma cells in large blood vessels in mice by using the intrinsic photoacoustic signal of melanin, and by targeting the tumor cells with magnetic nanoparticles (148). McCormack et al. used targeted gold nanoparticles to increase the signal from melanoma cells in a stationary *in vitro* system (144). The same group was able to use targeted gold nanoparticles in a breast cancer cell line and detect the non-pigmented circulating tumor cells with their system. Although they did not specifically show the detection of individual cells due to cell clumping, they claim that their system may be capable of this in clinical samples (149). Label-free or targeted photoacoustic CTC detection methods may be translated into human studies in the near future. Possible clinical applications to be evaluated include blood screening for early CTCs before the development of metastases to predict patient prognosis; testing for disease recurrence and individualized treatment monitoring through CTC counting; evaluation of surgical margins for CTCs; and even the inhibition/prevention of the development of metastases through therapeutic elimination of CTCs (150).

In addition to tumor cell detection in the circulation, photoacoustic imaging may also be very useful for visualization of the vessel wall itself, as several reports on atherosclerotic plaque characterization illustrate (37, 151, 152). Catheters that integrate intravascular ultrasound (IVUS) and intravascular photoacoustic (IVPA) imaging have been designed to approach tissues of interest through the blood vessels (153-159). In the future, these types of catheters could be used during intravascular procedures in a cardiovascular disease setting (e.g., coronary plaque characterization and stent placement), but possibly also in an oncologic setting (e.g., guidance of intravascular drug delivery directly to the tumor site).

Ophthalmic imaging

Ultrasound (US), optical coherence tomography (OCT) and fluorescent angiography play an important role in diagnostic imaging of the eye. Since PAI depicts optical absorption, which is independent of the tissue characteristics imaged by OCT or US, this technique can provide additional physiological information in ocular imaging. The eye is a very suitable application for optical imaging due to its accessibility and optical properties. The major light absorbing molecules in the eye are melanin and hemoglobin. Melanin is present in the uvea (iris, choroid, ciliary body) and in pigmented tumors, while hemoglobin is present in the abundant microvasculature of the uveal tract, in superficial microvessels of the eye (retina, conjunctiva) and in pathologic neovascularization (including tumors). The physiological information provided by PAI, for example changes in microcirculation, hypoxia, and nevi formation, could prove highly valuable in the diagnosis of ocular disease. Not only for the detection and characterization of cancer of the eye (e.g., intraocular melanoma, lymphoma, retinoblastoma, metastases), but also for other blinding diseases such as diabetic retinopathy, age-related macular degeneration, and glaucoma. To date several efforts have been made to develop PAI methods suitable for ophthalmologic applications, although so far only tested in experimental settings. Our labs have developed a photoacoustic ocular imaging device and demonstrated its utility in imaging in living rabbits the deeper layers of the eye including the retina, choroid, and optic nerve, Figure 10 (160). The Wang group has shown label-free photoacoustic angiography of the eye in mice (161). This is an alternative to the commonly used fluorescence angiography that requires injection of an imaging agent (fluorescein or indocyanine green), which may have side effects. The Zhang group has built several photoacoustic imaging platforms for ophthalmic imaging in rodents, including hybrid systems that combine photoacoustic ophthalmoscopy with other techniques such as optical coherence tomography and fluorescence imaging (162-165). Nevertheless, there is a need for further optimization and evaluation of ocular PAI systems before they can be tested in humans and evaluated against existing diagnostic techniques.

Bone and joint imaging

Peripheral joint imaging seems to be a highly accessible and promising area for PAI, as demonstrated in several pilot studies of human finger joints (166-169). In combination with conventional US, dual-modality imaging can potentially provide both morphological and physiological information on joints, such as blood flow, blood volume, hemoglobin oxygenation, and vascular density. It would be an advantage to be able to show that PAI early on can visualize the physiological changes in the articular tissue appearing before the late morphological changes. This would help to diagnose and treat joint disease at an earlier stage before it has become more manifest. Additionally, by visualizing these physiological features, PAI may be able to play a role in the diagnosis of primary bone cancer or bone metastases. A first study by Hu and colleagues demonstrated *in vivo* photoacoustic imaging of osteosarcoma in a rat leg, monitoring tumor development and showing apparent changes in imaging characteristics over the course of two weeks after cell injection (170). Although these initial results are encouraging, more research is needed to verify findings in human

studies and to overcome certain critical challenges of photoacoustic imaging, such as the limited depth penetration in bone (even more limited than in soft tissue).

Neonatal brain imaging

Ultrasound imaging is an established pediatric brain imaging modality that is used before the fontanelles are closed. After the closure of the fontanelles, the image quality degrades significantly because the skull severely attenuates and scatters ultrasonic waves. Transcranial ultrasonic brain imaging of adults is also limited by the inhomogeneous aberrating effect of the skull bone. Yang et al. applied photoacoustic tomography (PAT) to image the brain cortex of a monkey through the intact scalp and skull *ex vivo*. The reconstructed PAT image showed the major blood vessels on the monkey brain cortex (171). Because the human skull scatters light strongly, the same group added a photon recycler to the PAT system, to reflect back-scattered light back to the skull which in turn increased light transmittance through the skull (172). Recently Sussman et al. used PAT in a neonatal rat model to demonstrate *in vivo* alterations in cerebral hemodynamics in a non-invasive and near real-time fashion (173). These results suggest that PAT may have the potential for human brain cortex imaging in infants or even adults although further technical development is needed before proceeding to humans.

Gastrointestinal imaging

Endoscopic imaging is the main diagnostic tool in gastrointestinal diseases. Mostly, endoscopic imaging relies on wide-field white-light optical methods, which are limited by what the human eye can see and therefore lack sensitivity to subsurface or physiologic changes. Attempts to overcome these limitations include techniques such as autofluorescence imaging, narrow-band imaging, and optical coherence tomography (174, 175). Photoacoustic endoscopic imaging may have the ability to visualize physiologic processes and to resolve molecular imaging agents that target specific molecular changes in tissue. Subsurface imaging is well possible with this technique because of the favorable penetration depth (up to several centimeters). The combination of deeper tissue penetration, high resolution, and real-time imaging makes photoacoustic imaging a valuable add-on to endoscopy. It may allow for the detection of very small lesions (e.g., micro-metastases) or otherwise invisible “flat” lesions, probably even more so with the use of targeted molecular imaging agents. Intraoperatively, PAI could help in determining the extent of the tumor before surgical removal, and the completeness of the excision could be checked immediately. Also, this technique could assist in guiding the anastomosis procedures.

Only a few studies have been published in this application area. Recently, Yang and colleagues presented their endoscopy device that can acquire photoacoustic and ultrasonic data simultaneously. This device was tested *in vivo* in rabbit esophagi and in rat colons. With this technique, the esophagus and surrounding organs could be visualized, including the adjacent vasculature that was only visible in photoacoustic mode. Also, the vasculature in the colon wall could be seen, and after injection of Evans blue dye, the adjacent lymph structures became visible. Moreover, differences in oxygen saturation values could be indicated between the aorta and caudal vena cava in the rabbits (176). The groups of Yuan and Sheaff both describe a preclinical photoacoustic endoscope that they are developing (177, 178). The endoscope built by Yuan and colleagues was able to discriminate cancerous human colorectal tissue from normal human colorectal tissue *ex vivo*, with contrast ratios of ~2 (177). No clinical studies have been performed yet.

Thyroid imaging

Follicular thyroid carcinomas cannot be distinguished from adenomas based on their clinical, imaging, or cytological assessment, but always require surgical biopsy for

diagnosis. Since the majority of nodules (3/4) are benign, the need for new noninvasive detection methods to avoid unnecessary surgeries is clear, and photoacoustic imaging may be a valid candidate. To date, there are no studies published on photoacoustic thyroid imaging, but this application is currently under exploration by our research group (36). We developed an enzyme activatable photoacoustic probe that was previously described in this review (35). The presence and activity of two members of the matrix metalloproteinase family (MMP), MMP-2 and MMP-9, suggested to differentiate between malignant and benign lesions, were studied in a thyroid tumor mouse model. *In vivo* photoacoustic imaging results showed significantly higher signal in tumors injected with the enzyme activatable probe than in tumors injected with the control (non-cleavable) probe, indicating the probe's potential to distinguish between benign adenomas and MMP rich follicular carcinomas. We believe that with the combination of high spatial resolution and signal specificity, molecular photoacoustic imaging holds great promise as a noninvasive method for early diagnosis of follicular thyroid carcinomas.

Intraoperative Imaging

Intraoperative is another area where PAI has great potential, particularly because it can help the surgeon to see immediately beyond the resection surface. A portable PAI could be brought into the operating room and provide real-time images similar to intraoperative US. However, the optical contrast provides additional information over US images and could for instance help assess oxygen saturation and perfusion status of an organ (viability), useful in e.g., bowel resections, organ transplants, and amputations. Surgical resection also plays a critical role in the treatment of many cancers. It is of ultimate importance to reassure complete resection of the tumor mass in order to diminish the risk for local recurrence and improve survival rates. CT, MRI, or PET-CT imaging (depending on tumor type) can give information on tumor extent before surgery, but during the operative procedure the surgeon currently relies on visual appearance and palpation. Several intraoperative imaging methods have been evaluated, such as ultrasound and intraoperative MRI, but they have been found either too time consuming or lacking sufficient spatial resolution. PAI could potentially provide a solution to this problem. The exploration of PAI in the intraoperative setting is still in its infancy. Xi et al. report a microelectromechanical systems based intraoperative PAT (iPAT) technique, and demonstrate its ability to accurately map tumors in three-dimensions and to inspect the completeness of tumor resection during surgery in a tumor-bearing mouse model (179). They propose potential use of the iPAT technique in breast cancer surgery although they point out the need for development of a handheld probe with increased depth resolution before clinical translation of the technique. Furthermore, to deal with the strong effect of blood (from intraoperative bleeding) on PAI absorption they suggest use of targeted molecular imaging agents to provide enough contrast. In a recent review, Su et al. discuss potential future intraoperative imaging methods for malignant gliomas, a common type of brain tumor. Among other techniques, they point out that PAI in combination with optical imaging agents could be promising (180). This application has been explored by our lab, with the development of a triple-modality Magnetic resonance imaging-Photoacoustic imaging-Raman imaging nanoparticle that can accurately help delineate the margins of brain tumors in living mice both preoperatively and intraoperatively (86) (see also Figure 5)

Besides tumor delineation and assessment of its margins, PAI could also play a role in the assessment of metastases, in particular the lymph node status. Earlier on, we discussed the sentinel lymph node procedure for breast cancer. The lymph node status for other types of cancer could also be explored by PAI during tumor resection, for instance in the case of an abdominal tumor, the surgeon would be able to make quick decisions on the resection of suspicious (mesenteric) lymph nodes during laparotomy or laparoscopy. For this situation

most likely an imaging agent would have to be injected to provide enough sensitivity and specificity. Grootendorst et al. have shown in healthy rats that superparamagnetic iron oxide nanoparticles (Endorem(®)) can be used as a photoacoustic imaging agent for lymph node visualization (87). More recently, they have shown promising results using the same nanoparticles in an *ex vivo* intraoperative setting in a metastatic prostate cancer model in rats (181).

Combination of diagnostics and therapy—PAI (combined with other modalities) could also be used in a clinical setting to guide treatment and to combine diagnostic information with therapy ("theranostics"). Photoacoustic imaging has recently been proposed to guide and/or monitor therapy based on high-intensity focused ultrasound (HIFU) (182). Prost et al. show a lesion obtained *in vitro* in chicken breast by focusing HIFU based on the photoacoustic signals emitted by an optical absorber placed in the tissue (183). Gold-nanoparticle mediated hyperthermia shows particular promise in animal studies and is currently being investigated in early clinical studies (184). The visualization and tracking of temporarily or permanently implanted metal devices, such as biopsy needles and needles used for localized drug delivery, have been studied with PAI (185). The results suggest that photoacoustic imaging, combined with ultrasound imaging, is capable of real-time, high contrast, and high spatial resolution visualization of metal implants within anatomical landmarks of the background tissue.

Outlook

Photoacoustic imaging holds the promise of becoming a valuable tool in multiple clinical areas in which there are unmet needs. This technique has several important strengths over the currently available imaging techniques; in particular its ability to obtain functional and molecular information from tissue, even without the use of a molecular imaging agent, but also its low cost, portability, lack of ionizing radiation, and feasibility of real-time imaging at high resolution and clinically relevant depths. PAI can be utilized not only in a non-invasive way, but also in an intraoperative or endoscopic imaging setting. The combination of PAI with existing imaging techniques (multi-modality imaging) or delivery of therapeutics will likely add even more to its potential.

Besides these major advantages, there are still important challenges to overcome. Clinicians will need to get familiar with the photoacoustic imaging technique and become aware of its capabilities and limitations. The most obvious limitation for clinical applications of PAI is its penetration depth, dependent on the limited penetration of light in tissue, which will likely not reach beyond several cm (~7 cm, Table 1) in the near-infrared wavelength range. Since spatial resolution is associated with penetration depth in PAI, the detection of smaller lesions (a few mm) located deeper in the tissue will need to be investigated. As for the propagation of ultrasound waves in tissue, the same limitations apply as in ultrasound imaging, i.e., limited penetration through bone and air.

Although the photoacoustic imaging technology has already reached a level that can be used in clinical studies, there is still much room for improvement. Fast, tunable systems that can provide multispectral images in real-time should be developed, and photoacoustic imaging systems need to become stable and user-friendly with regard to data acquisition and analysis; in particular progress in quantitative data analysis is essential. The development of miniaturized probes is needed for endoscopic, intravesicular and intravascular PAI. For intravascular clinical use, the photoacoustic probe should be scaled down to < 1 mm in diameter (186).

Image contrast and sensitivity of detection represent another area of needed improvement for PAI. Since one of the main advantages of photoacoustic imaging is that endogenous chromophores can be imaged without the injection of an exogenous imaging agent, this intrinsic contrast will most likely be the primary focus of initial clinical studies. Therefore, we will need to learn more about the distribution of intrinsic features, such as neoangiogenesis and hypoxia/oxygen saturation, within and between the various cancer types and benign lesions. Tumors that are less vascularized could be a caveat, but overall this intrinsic contrast may provide us with substantial functional information on tissue. To enhance photoacoustic image contrast, exogenous molecular imaging agents are under development and will need to be approved for use in humans. Several key concerns regarding these molecular imaging agents remain. These include (1) the ability to produce sufficient PAI signal with a relatively low dose of injected imaging agent. It may be the case that for some agents, insufficient amounts can be delivered to the target site(s) because of limits in the total mass that can be injected while still being non-toxic to the subject. (2) Regulatory issues that have held up the translation of optical imaging agents will likely slow down the clinical translation of photoacoustic imaging agents as well. (3) The ability to show the added value of using an imaging agent in addition to intrinsic PAI signal will have to be carefully studied. Nevertheless, once relevant molecular imaging agents become available for clinical PAI, this technique may play an even more significant role in a variety of diseases with respect to their detection, staging, treatment planning and monitoring (see also Figure 3).

In conclusion, the recent surge in interest in photoacoustic imaging has provided us with a wealth of experience and knowledge from preclinical studies. Promising results and technological advances lay the foundation for clinical translation of this technique. Although challenges remain, few of them are beyond reach. Further developments in laser sources and detectors, image processing algorithms, and molecular imaging agents, will open up opportunities for photoacoustic imaging in disease detection, treatment surveillance, and targeted therapy in a range of pathologies. Its ability for high resolution molecular imaging in real-time, its nonionizing properties, and its compatibility with existing imaging systems (US in particular), will help strengthen PAI's position in the fast-growing imaging arena in the near future.

Supplementary Material

Refer to Web version on PubMed Central for supplementary material.

References

1. Bell AG. On the production of sound by light. Am J Sci. 1880; 20(305)
2. Zhang HF, Maslov K, Stoica G, Wang LV. Functional photoacoustic microscopy for high-resolution and noninvasive in vivo imaging. Nat Biotechnol. 2006; 24(7):848–51. [PubMed: 16823374]
3. Ku G, Wang LV. Deeply penetrating photoacoustic tomography in biological tissues enhanced with an optical contrast agent. Opt Lett. 2005; 30(5):507–9. [PubMed: 15789718]
4. Emelianov SYA, Karpiouk SR, Mallidi AB, Park S, Sethuraman S, Shah S, Smalling J, Rubin RW, Scott JM. W.G. Synergy and Applications of Combined Ultrasound, Elasticity, and Photoacoustic Imaging. IEEE Int UltrasonSymp [Internet]. 2006
5. Maslov K, Zhang HF, Hu S, Wang LV. Optical-resolution photoacoustic microscopy for in vivo imaging of single capillaries. Opt Lett. 2008; 33(9):929–31. [PubMed: 18451942]
6. Wang LV, Hu S. Photoacoustic tomography: in vivo imaging from organelles to organs. Science (New York, NY). 2012; 335(6075):1458–62.

7. Kim C, Erpelding TN, Jankovic L, Pashley MD, Wang LV. Deeply penetrating in vivo photoacoustic imaging using a clinical ultrasound array system. Biomed Opt Express. 2010; 1(1): 278–84. [PubMed: 21258465]
8. Manohar S, Vaartjes SE, van Hespen JC, Klaase JM, van den Engh FM, Steenbergen W, et al. Initial results of in vivo non-invasive cancer imaging in the human breast using near-infrared photoacoustics. Opt Express. 2007; 15(19):12277–85. [PubMed: 19547596]
9. Kruger RA, Lam RB, Reinecke DR, Del Rio SP, Doyle RP. Photoacoustic angiography of the breast. Med Phys. 2010; 37(11):6096–100. [PubMed: 21158321]
10. Esenaliev JK, Oraevsky AA. A.A. Sensitivity of laser opto-acoustic imaging in detection of small deeply embedded tumors. IEEE J Selected Top Quantum Electron. 1999; 5:981–88.
11. Wang LV. Multiscale photoacoustic microscopy and computed tomography. Nat Photonics. 2009; 3(9):503–09. [PubMed: 20161535]
12. Su JL, Wang B, Wilson KE, Bayer CL, Chen YS, Kim S, et al. Advances in Clinical and Biomedical Applications of Photoacoustic Imaging. Expert Opin Med Diagn. 2010; 4(6):497–510. [PubMed: 21344060]
13. Kruger RA, Kiser WL Jr. Reinecke DR, Kruger GA. Thermoacoustic computed tomography using a conventional linear transducer array. Med Phys. 2003; 30(5):856–60. [PubMed: 12772993]
14. Yin B, Xing D, Wang Y, Zeng Y, Tan Y, Chen Q. Fast photoacoustic imaging system based on 320-element linear transducer array. Phys Med Biol. 2004; 49(7):1339–46. [PubMed: 15128209]
15. Kothapalli S, Ma T, Vaithilingam S, Oralkan O, Khuri-Yakub B, Gambhir S. Deep Tissue Photoacoustic Imaging Using a Miniaturized 2-D Capacitive Micromachined Ultrasonic Transducer Array. IEEE Trans Biomed Eng. 2012
16. Zemp RJ, Bitton R, Li ML, Shung KK, Stoica G, Wang LV. Photoacoustic imaging of the microvasculature with a high-frequency ultrasound array transducer. J Biomed Opt. 2007; 12(1): 010501. [PubMed: 17343475]
17. Li C, Wang LV. Photoacoustic tomography and sensing in biomedicine. Phys Med Biol. 2009; 54(19):R59–97. [PubMed: 19724102]
18. Gibson AP, Hebden JC, Arridge SR. Recent advances in diffuse optical imaging. Phys Med Biol. 2005; 50(4):R1–43. [PubMed: 15773619]
19. Schulze R, Zangerl G, Holotta M, Meyer D, Handle F, Nuster R, et al. On the use of frequency-domain reconstruction algorithms for photoacoustic imaging. J Biomed Opt. 2011; 16(8):086002. [PubMed: 21895314]
20. Xia J, Guo Z, Maslov K, Aguirre A, Zhu Q, Percival C, et al. Three-dimensional photoacoustic tomography based on the focal-line concept. J Biomed Opt. 2011; 16(9):090505. [PubMed: 21950908]
21. Yao L, Jiang H. Photoacoustic image reconstruction from few-detector and limited-angle data. Biomed Opt Express. 2011; 2(9):2649–54. [PubMed: 21991554]
22. Zhu B, Sevick-Muraca EM. Reconstruction of sectional images in frequency-domain based photoacoustic imaging. Opt Express. 2011; 19(23):23286–97. [PubMed: 22109207]
23. Sheu YL, Chou CY, Hsieh BY, Li PC. Image reconstruction in intravascular photoacoustic imaging. IEEE Trans Ultrason Ferroelectr Freq Control. 2011; 58(10):2067–77. [PubMed: 21989871]
24. Oraevsky, A.; Karabutov, A. Optoacoustic tomography.. In: Vo-Dinh, T., editor. Biomedical Photonics Handbook. CRC Press; 2003.
25. Wang, LV.; Wu, H.i. Biomedical Optics: Principles and Imaging. Wiley; Hoboken, NJ: 2007.
26. Wang LV. Prospects of photoacoustic tomography. Med Phys. 2008; 35(12):5758–67. [PubMed: 19175133]
27. Xu MH, Wang LH. Photoacoustic imaging in biomedicine. Rev Sci Instrum. 2006; 77(041101)
28. Emelianov SY, Li PC, O'Donnell M. Photoacoustics for molecular imaging and therapy. Phys Today. 2009; 62(8):34–39. [PubMed: 20523758]
29. Rice A, Quinn CM. Angiogenesis, thrombospondin, and ductal carcinoma in situ of the breast. J Clin Pathol. 2002; 55(8):569–74. [PubMed: 12147647]

30. Wang B, Su JL, Amirian J, Litovsky SH, Smalling R, Emelianov S. Detection of lipid in atherosclerotic vessels using ultrasound-guided spectroscopic intravascular photoacoustic imaging. Opt Express. 2010; 18(5):4889–97. [PubMed: 20389501]

31. Ermilov SA, Khamapirad T, Conjusteau A, Leonard MH, Lacewell R, Mehta K, et al. Laser optoacoustic imaging system for detection of breast cancer. J Biomed Opt. 2009; 14(2):024007. [PubMed: 19405737]

32. Kumon RE, Deng CX, Wang X. Frequency-domain analysis of photoacoustic imaging data from prostate adenocarcinoma tumors in a murine model. Ultrasound Med Biol. 2011; 37(5):834–9. [PubMed: 21376447]

33. Bhattacharyya S, Wang S, Reinecke D, Kiser W Jr. Kruger RA, DeGrado TR. Synthesis and evaluation of near-infrared (NIR) dye-herceptin conjugates as photoacoustic computed tomography (PCT) probes for HER2 expression in breast cancer. Bioconjug Chem. 2008; 19(6): 1186–93. [PubMed: 18505279]

34. Yang Q, Cui H, Cai S, Yang X, Forrest ML. In vivo photoacoustic imaging of chemotherapy-induced apoptosis in squamous cell carcinoma using a near-infrared caspase-9 probe. J Biomed Opt. 16(11):116026. [PubMed: 22112131]

35. Levi J, Kothapalli SR, Ma TJ, Hartman K, Khuri-Yakub BT, Gambhir SS. Design, synthesis, and imaging of an activatable photoacoustic probe. J Am Chem Soc. 2010; 132(32):11264–9. [PubMed: 20698693]

36. Levi J, Kothapalli SR, Bohndiek S, Yoon JK, Dragulescu-Andrasi A, Nielsen C, et al. Molecular photoacoustic imaging of follicular thyroid carcinoma. Clin Cancer Res. 2013; 19(6):1494–502. [PubMed: 23349314]

37. Razansky D, Harlaar NJ, Hillebrands JL, Taruttis A, Herzog E, Zeebregts CJ, et al. Multispectral Optoacoustic Tomography of Matrix Metalloproteinase Activity in Vulnerable Human Carotid Plaques. Mol Imaging Biol.

38. Kim C, Song KH, Gao F, Wang LV. Sentinel lymph nodes and lymphatic vessels: noninvasive dual-modality in vivo mapping by using indocyanine green in rats--volumetric spectroscopic photoacoustic imaging and planar fluorescence imaging. Radiology. 2010; 255(2):442–50. [PubMed: 20413757]

39. Wang X, Ku G, Wegiel MA, Bornhop DJ, Stoica G, Wang LV. Noninvasive photoacoustic angiography of animal brains in vivo with near-infrared light and an optical contrast agent. Opt Lett. 2004; 29(7):730–2. [PubMed: 15072373]

40. Song KH, Stein EW, Margenthaler JA, Wang LV. Noninvasive photoacoustic identification of sentinel lymph nodes containing methylene blue in vivo in a rat model. J Biomed Opt. 2008; 13(5):054033. [PubMed: 19021413]

41. Song L, Kim C, Maslov K, Shung KK, Wang LV. High-speed dynamic 3D photoacoustic imaging of sentinel lymph node in a murine model using an ultrasound array. Med Phys. 2009; 36(8):3724–9. [PubMed: 19746805]

42. Li C, Aguirre A, Gamelin J, Maurudis A, Zhu Q, Wang LV. Real-time photoacoustic tomography of cortical hemodynamics in small animals. J Biomed Opt. 2010; 15(1):010509. [PubMed: 20210422]

43. Li M, Oh JT, Xie X, Ku G, Wang W, Li C, et al. Simultaneous Molecular and Hypoxia Imaging of Brain Tumors In Vivo Using Spectroscopic Photoacoustic Tomography. Proceedings of the IEEE. 2008; 96(3):481–89.

44. Kim G, Huang SW, Day KC, O'Donnell M, Agayan RR, Day MA, et al. Indocyanine-green-embedded PEBBLEs as a contrast agent for photoacoustic imaging. J Biomed Opt. 2007; 12(4): 044020. [PubMed: 17867824]

45. Gupta S, Chatni MR, Rao AL, Vullev VI, Wang LV, Anvari B. Virus-mimicking nano-constructs as a contrast agent for near infrared photoacoustic imaging. Nanoscale. 2013; 5(5):1772–6. [PubMed: 23334567]

46. Bayer CL, Chen YS, Kim S, Mallidi S, Sokolov K, Emelianov S. Multiplex photoacoustic molecular imaging using targeted silica-coated gold nanorods. Biomed Opt Express. 2(7):1828–35. [PubMed: 21750761]

47. Xie H, Diagaradjane P, Deorukhkar AA, Goins B, Bao A, Phillips WT, et al. Integrin alphavbeta3-targeted gold nanoshells augment tumor vasculature-specific imaging and therapy. Int J Nanomedicine. 6:259–69. [PubMed: 21423588]
48. Li ML, Wang JC, Schwartz JA, Gill-Sharp KL, Stoica G, Wang LV. In-vivo photoacoustic microscopy of nanoshell extravasation from solid tumor vasculature. J Biomed Opt. 2009; 14(1): 010507. [PubMed: 19256687]
49. Eghtedari M, Liopo AV, Copland JA, Oraevsky AA, Motamedi M. Engineering of hetero-functional gold nanorods for the in vivo molecular targeting of breast cancer cells. Nano Lett. 2009; 9(1):287–91. [PubMed: 19072129]
50. Eghtedari M, Oraevsky A, Copland JA, Kotov NA, Conjusteau A, Motamedi M. High sensitivity of in vivo detection of gold nanorods using a laser optoacoustic imaging system. Nano Lett. 2007; 7(7):1914–8. [PubMed: 17570730]
51. Li PC, Wang CR, Shieh DB, Wei CW, Liao CK, Poe C, et al. In vivo photoacoustic molecular imaging with simultaneous multiple selective targeting using antibody-conjugated gold nanorods. Opt Express. 2008; 16(23):18605–15. [PubMed: 19581946]
52. Copland JA, Eghtedari M, Popov VL, Kotov N, Mamedova N, Motamedi M, et al. Bioconjugated gold nanoparticles as a molecular based contrast agent: implications for imaging of deep tumors using optoacoustic tomography. Mol Imaging Biol. 2004; 6(5):341–9. [PubMed: 15380744]
53. Kim C, Cho EC, Chen J, Song KH, Au L, Favazza C, et al. In vivo molecular photoacoustic tomography of melanomas targeted by bioconjugated gold nanocages. ACS Nano. 2010; 4(8): 4559–64. [PubMed: 20731439]
54. Skrabalak SE, Chen J, Sun Y, Lu X, Au L, Cobley CM, et al. Gold nanocages: synthesis, properties, and applications. Acc Chem Res. 2008; 41(12):1587–95. [PubMed: 18570442]
55. Yang X, Skrabalak SE, Li ZY, Xia Y, Wang LV. Photoacoustic tomography of a rat cerebral cortex in vivo with au nanocages as an optical contrast agent. Nano Lett. 2007; 7(12):3798–802. [PubMed: 18020475]
56. Jokerst JV, Thangaraj M, Kempen PJ, Sinclair R, Gambhir SS. Photoacoustic Imaging of Mesenchymal Stem Cells in Living Mice via Silica-Coated Gold Nanorods. ACS Nano. 2012
57. Jokerst JV, Cole AJ, Van de Sompel D, Gambhir SS. Gold nanorods for ovarian cancer detection with photoacoustic imaging and resection guidance via Raman imaging in living mice. ACS Nano. 2012; 6(11):10366–77. [PubMed: 23101432]
58. Kim C, Song HM, Cai X, Yao J, Wei A, Wang LV. In vivo photoacoustic mapping of lymphatic systems with plasmon-resonant nanostars. J Mater Chem. 2011; 21(9):2841–44. [PubMed: 21660122]
59. Ma LL, Feldman MD, Tam JM, Paranjape AS, Cheruku KK, Larson TA, et al. Small multifunctional nanoclusters (nanoroses) for targeted cellular imaging and therapy. ACS Nano. 2009; 3(9):2686–96. [PubMed: 19711944]
60. Ma LL, Tam JO, Willsey BW, Rigdon D, Ramesh R, Sokolov K, et al. Selective targeting of antibody conjugated multifunctional nanoclusters (nanoroses) to epidermal growth factor receptors in cancer cells. Langmuir. 27(12):7681–90. [PubMed: 21591638]
61. Bouchard LS, Anwar MS, Liu GL, Hann B, Xie ZH, Gray JW, et al. Picomolar sensitivity MRI and photoacoustic imaging of cobalt nanoparticles. Proc Natl Acad Sci U S A. 2009; 106(11): 4085–9. [PubMed: 19251659]
62. Yoon SJ, Mallidi S, Tam JM, Tam JO, Murthy A, Johnston KP, et al. Utility of biodegradable plasmonic nanoclusters in photoacoustic imaging. Opt Lett. 35(22):3751–3. [PubMed: 21081985]
63. Chen YS, Frey W, Kim S, Homan K, Kruizinga P, Sokolov K, et al. Enhanced thermal stability of silica-coated gold nanorods for photoacoustic imaging and image-guided therapy. Opt Express. 18(9):8867–78. [PubMed: 20588732]
64. Chen YS, Frey W, Kim S, Kruizinga P, Homan K, Emelianov S. Silica-coated gold nanorods as photoacoustic signal nanoamplifiers. Nano Lett. 11(2):348–54. [PubMed: 21244082]
65. Zhang B, Fang CY, Chang CC, Peterson R, Maswadi S, Glickman RD, et al. Photoacoustic emission from fluorescent nanodiamonds enhanced with gold nanoparticles. Biomed Opt Express. 2012; 3(7):1662–29. [PubMed: 22808436]

66. Zhang T, Cui H, Fang CY, Su LJ, Ren S, Chang HC, et al. Photoacoustic contrast imaging of biological tissues with nanodiamonds fabricated for high near-infrared absorbance. J Biomed Opt. 2013; 18(2):26018. [PubMed: 23400417]

67. Pramanik M, Swierczewska M, Green D, Sitharaman B, Wang LV. Single-walled carbon nanotubes as a multimodal-thermoacoustic and photoacoustic-contrast agent. J Biomed Opt. 2009; 14(3):034018. [PubMed: 19566311]

68. De la Zerda A, Liu Z, Bodapati S, Teed R, Vaithilingam S, Khuri-Yakub BT, et al. Ultrahigh sensitivity carbon nanotube agents for photoacoustic molecular imaging in living mice. Nano Lett. 2010; 10(6):2168–72. [PubMed: 20499887]

69. De la Zerda A, Zavaleta C, Keren S, Vaithilingam S, Bodapati S, Liu Z, et al. Carbon nanotubes as photoacoustic molecular imaging agents in living mice. Nat Nanotechnol. 2008; 3(9):557–62. [PubMed: 18772918]

70. Koo J, Jeon M, Oh Y, Kang HW, Kim J, Kim C, et al. In vivo non-ionizing photoacoustic mapping of sentinel lymph nodes and bladders with ICG-enhanced carbon nanotubes. Phys Med Biol. 2012; 57(23):7853–62. [PubMed: 23151772]

71. Kim JW, Galanzha EI, Shashkov EV, Moon HM, Zharov VP. Golden carbon nanotubes as multimodal photoacoustic and photothermal high-contrast molecular agents. Nat Nanotechnol. 2009; 4(10):688–94. [PubMed: 19809462]

72. Shashkov EV, Everts M, Galanzha EI, Zharov VP. Quantum dots as multimodal photoacoustic and photothermal contrast agents. Nano Lett. 2008; 8(11):3953–8. [PubMed: 18834183]

73. Ku G, Zhou M, Song S, Huang Q, Hazle J, Li C. Copper sulfide nanoparticles as a new class of photoacoustic contrast agent for deep tissue imaging at 1064 nm. ACS Nano. 2012; 6(8):7489–96. [PubMed: 22812694]

74. Wick P, Clift MJ, Rosslein M, Rothen-Rutishauser B. A brief summary of carbon nanotubes science and technology: a health and safety perspective. ChemSusChem. 4(7):905–11. [PubMed: 21728250]

75. Schipper ML, Nakayama-Ratchford N, Davis CR, Kam NW, Chu P, Liu Z, et al. A pilot toxicology study of single-walled carbon nanotubes in a small sample of mice. Nat Nanotechnol. 2008; 3(4):216–21. [PubMed: 18654506]

76. Altinoglu EI, Russin TJ, Kaiser JM, Barth BM, Eklund PC, Kester M, et al. Near-infrared emitting fluorophore-doped calcium phosphate nanoparticles for in vivo imaging of human breast cancer. ACS Nano. 2008; 2(10):2075–84. [PubMed: 19206454]

77. Bottrill M, Green M. Some aspects of quantum dot toxicity. Chem Commun (Camb). 47(25):7039–50. [PubMed: 21475767]

78. Fernandez-Fernandez A, Manchanda R, McGoron AJ. Theranostic applications of nanomaterials in cancer: drug delivery, image-guided therapy, and multifunctional platforms. Appl Biochem Biotechnol. 165(7-8):1628–51. [PubMed: 21947761]

79. Yavuz MS, Cheng Y, Chen J, Cobley CM, Zhang Q, Rycenga M, et al. Gold nanocages covered by smart polymers for controlled release with near-infrared light. Nat Mater. 2009; 8(12):935–9. [PubMed: 19881498]

80. Wang C, Chen J, Talavage T, Irudayaraj J. Gold nanorod/Fe3O4 nanoparticle “nano-pearl-necklaces” for simultaneous targeting, dual-mode imaging, and photothermal ablation of cancer cells. Angew Chem Int Ed Engl. 2009; 48(15):2759–63. [PubMed: 19283813]

81. Jin Y, Jia C, Huang SW, O'Donnell M, Gao X. Multifunctional nanoparticles as coupled contrast agents. Nat Commun. 2010; 1:41. [PubMed: 20975706]

82. Qu M, Mallidi S, Mehrmohammadi M, Truby R, Homan K, Joshi P, et al. Magneto-photo-acoustic imaging. Biomed Opt Express. 2011; 2(2):385–96. [PubMed: 21339883]

83. Kim C, Qin R, Xu JS, Wang LV, Xu R. Multifunctional microbubbles and nanobubbles for photoacoustic and ultrasound imaging. J Biomed Opt. 2010; 15(1):010510. [PubMed: 20210423]

84. Wilson K, Homan K, Emelianov S. Biomedical photoacoustics beyond thermal expansion using triggered nanodroplet vaporization for contrast-enhanced imaging. Nat Commun. 2012; 3:618. [PubMed: 22233628]

85. Agarwal A, Shao X, Rajian JR, Zhang H, Chamberland DL, Kotov NA, et al. Dual-mode imaging with radiolabeled gold nanorods. J Biomed Opt. 2011; 16(5):051307. [PubMed: 21639567]

86. Kircher MF, De la Zerda A, Jokerst J, Zavaleta CL, Kempen P, Mittra E, Pitter K, Huang R, Campos C, Habte F, Sinclair R, Brennan C, Mellinghoff IK, Holland E, Gambhir SS. A Brain Tumor Molecular Imaging Strategy Using a Novel Triple-Modality Nanoparticle. Nature Medicine. 2012; 18(5):829–34.
87. Grootendorst DJ, Jose J, Fratila RM, Visscher M, Velders AH, Ten Haken B, et al. Evaluation of superparamagnetic iron oxide nanoparticles (Endorem(R)) as a photoacoustic contrast agent for intra-operative nodal staging. Contrast media & molecular imaging. 2013; 8(1):83–91. [PubMed: 23109396]
88. Li L, Zhang HF, Zemp RJ, Maslov K, Wang L. Simultaneous imaging of a lacZ-marked tumor and microvasculature morphology in vivo by dual-wavelength photoacoustic microscopy. Journal of innovative optical health sciences. 2008; 1(2):207–15. [PubMed: 19946613]
89. Cai X, Li L, Krumholz A, Guo Z, Erpelding TN, Zhang C, et al. Multi-scale molecular photoacoustic tomography of gene expression. PloS one. 2012; 7(8):e43999. [PubMed: 22952846]
90. Filonov GS, Krumholz A, Xia J, Yao J, Wang LV, Verkhusha VV. Deep-Tissue Photoacoustic Tomography of a Genetically Encoded Near-Infrared Fluorescent Probe. Angew Chem Int Ed Engl.
91. Ha SH, Carson AR, Kim K. Ferritin as a novel reporter gene for photoacoustic molecular imaging. Cytometry A. 2012; 81(10):910–5. [PubMed: 22949299]
92. Qin C, Cheng K, Chen K, Hu X, Liu Y, Lan X, et al. Tyrosinase as a multifunctional reporter gene for Photoacoustic/MRI/PET triple modality molecular imaging. Scientific reports. 2013; 3:1490. [PubMed: 23508226]
93. Kitai T, Torii M, Sugie T, Kanao S, Mikami Y, Shiina T, et al. Photoacoustic mammography: initial clinical results. Breast cancer (Tokyo, Japan). 2012
94. Heijblom M, Piras D, Xia W, van Hespen JC, Klaase JM, van den Engh FM, et al. Visualizing breast cancer using the Twente photoacoustic mammoscope: What do we learn from twelve new patient measurements? Opt Express. 2012; 20(11):11582–97. [PubMed: 22714144]
95. Manohar S, Kharine A, van Hespen JC, Steenbergen W, van Leeuwen TG. Photoacoustic mammography laboratory prototype: imaging of breast tissue phantoms. J Biomed Opt. 2004; 9(6):1172–81. [PubMed: 15568937]
96. Jose J, Manohar S, Kolkman RG, Steenbergen W, van Leeuwen TG. Imaging of tumor vasculature using Twente photoacoustic systems. J Biophotonics. 2009; 2(12):701–17. [PubMed: 19718681]
97. Haisch C, Eilert-Zell K, Vogel MM, Menzenbach P, Niessner R. Combined optoacoustic/ ultrasound system for tomographic absorption measurements: possibilities and limitations. Anal Bioanal Chem. 2010; 397(4):1503–10. [PubMed: 20383696]
98. Ku G, Fornage BD, Jin X, Xu M, Hunt KK, Wang LV. Thermoacoustic and photoacoustic tomography of thick biological tissues toward breast imaging. Technol Cancer Res Treat. 2005; 4(5):559–66. [PubMed: 16173826]
99. Pramanik M, Ku G, Li C, Wang LV. Design and evaluation of a novel breast cancer detection system combining both thermoacoustic (TA) and photoacoustic (PA) tomography. Med Phys. 2008; 35(6):2218–23. [PubMed: 18649451]
100. Xia W, Piras D, van Hespen JC, van Veldhoven S, Prins C, van Leeuwen TG, et al. An optimized ultrasound detector for photoacoustic breast tomography. Med Phys. 2013; 40(3):032901. [PubMed: 23464340]
101. Montilla LG, Olafsson R, Bauer DR, Witte RS. Real-time photoacoustic and ultrasound imaging: a simple solution for clinical ultrasound systems with linear arrays. Phys Med Biol. 2013; 58(1):N1–12. [PubMed: 23221479]
102. Cheng G, Kurita S, Torigian DA, Alavi A. Current status of sentinel lymph-node biopsy in patients with breast cancer. Eur J Nucl Med Mol Imaging. 2011; 38(3):562–75. [PubMed: 20700739]
103. Purushotham AD, Upponi S, Klevesath MB, Bobrow L, Millar K, Myles JP, et al. Morbidity after sentinel lymph node biopsy in primary breast cancer: results from a randomized controlled trial. Journal of clinical oncology : official journal of the American Society of Clinical Oncology. 2005; 23(19):4312–21. [PubMed: 15994144]

104. Crane-Okada R, Wascher RA, Elashoff D, Giuliano AE. Long-term morbidity of sentinel node biopsy versus complete axillary dissection for unilateral breast cancer. Annals of surgical oncology. 2008; 15(7):1996–2005. [PubMed: 18415650]

105. Song KH, Kim C, Cobley CM, Xia Y, Wang LV. Near-infrared gold nanocages as a new class of tracers for photoacoustic sentinel lymph node mapping on a rat model. Nano Lett. 2009; 9(1): 183–8. [PubMed: 19072058]

106. Erpelding TN, Kim C, Pramanik M, Jankovic L, Maslov K, Guo Z, et al. Sentinel lymph nodes in the rat: noninvasive photoacoustic and US imaging with a clinical US system. Radiology. 2010; 256(1):102–10. [PubMed: 20574088]

107. Kim C, Erpelding TN, Maslov K, Jankovic L, Akers WJ, Song L, et al. Handheld array-based photoacoustic probe for guiding needle biopsy of sentinel lymph nodes. J Biomed Opt. 2010; 15(4):046010. [PubMed: 20799812]

108. Akers WJ, Edwards WB, Kim C, Xu B, Erpelding TN, Wang LV, et al. Multimodal sentinel lymph node mapping with single-photon emission computed tomography (SPECT)/computed tomography (CT) and photoacoustic tomography. Translational research : the journal of laboratory and clinical medicine. 2012; 159(3):175–81. [PubMed: 22340767]

109. Heijmink SW, Futterer JJ, Strum SS, Oyen WJ, Frauscher F, Witjes JA, et al. State-of-the-art uroradiologic imaging in the diagnosis of prostate cancer. Acta Oncol. 2011; 50(Suppl 1):25–38. [PubMed: 21604938]

110. Ilic D, Neuberger MM, Djulbegovic M, Dahm P. Screening for prostate cancer. Cochrane database of systematic reviews (Online). 2013; 1:CD004720.

111. Oraevsky AA, Ermilov S, Metha K, Miller T, Bell B, Orihuela E, Motamedi M. In vivo Testing of Laser Optoacoustic System for Image-Guided Biopsy of Prostate. Proceedings of SPIE. 2006:6086.

112. Wang X, Roberts WW, Carson PL, Wood DP, Fowlkes JB. Photoacoustic tomography: a potential new tool for prostate cancer. Biomed Opt Express. 2010; 1(4):1117–26. [PubMed: 21258534]

113. Yaseen MA, Ermilov SA, Brecht HP, Su R, Conjusteau A, Fronheiser M, et al. Optoacoustic imaging of the prostate: development toward image-guided biopsy. J Biomed Opt. 2010; 15(2): 021310. [PubMed: 20459232]

114. Bauer DR, Olafsson R, Montilla LG, Witte RS. 3-D photoacoustic and pulse echo imaging of prostate tumor progression in the mouse window chamber. J Biomed Opt. 2011; 16(2):026012. [PubMed: 21361696]

115. Olafsson R, Bauer DR, Montilla LG, Witte RS. Real-time, contrast enhanced photoacoustic imaging of cancer in a mouse window chamber. Opt Express. 2010; 18(18):18625–32. [PubMed: 20940754]

116. Davis BJ, Horwitz EM, Lee WR, Crook JM, Stock RG, Merrick GS, et al. American Brachytherapy Society consensus guidelines for transrectal ultrasound-guided permanent prostate brachytherapy. Brachytherapy. 2012; 11(1):6–19. [PubMed: 22265434]

117. Yamada Y, Rogers L, Demanes DJ, Morton G, Prestidge BR, Pouliot J, et al. American Brachytherapy Society consensus guidelines for high-dose-rate prostate brachytherapy. Brachytherapy. 2012; 11(1):20–32. [PubMed: 22265435]

118. Su JL, Bouchard RR, Karpiouk AB, Hazle JD, Emelianov SY. Photoacoustic imaging of prostate brachytherapy seeds. Biomed Opt Express. 2011; 2(8):2243–54. [PubMed: 21833361]

119. Harrison T, Zemp RJ. Coregistered photoacoustic-ultrasound imaging applied to brachytherapy. J Biomed Opt. 2011; 16(8):080502. [PubMed: 21895302]

120. Kuo N, Kang HJ, Song DY, Kang JU, Boctor EM. Real-time photoacoustic imaging of prostate brachytherapy seeds using a clinical ultrasound system. J Biomed Opt. 2012; 17(6):066005. [PubMed: 22734761]

121. Xie Z, Roberts W, Carson P, Liu X, Tao C, Wang X. Evaluation of bladder microvasculature with high-resolution photoacoustic imaging. Opt Lett. 2011; 36(24):4815–7. [PubMed: 22179893]

122. Kim C, Jeon M, Wang LV. Nonionizing photoacoustic cystography in vivo. Opt Lett. 2011; 36(18):3599–601. [PubMed: 21931403]

123. Smith L, Macneil S. State of the art in non-invasive imaging of cutaneous melanoma. Skin Res Technol. 2011

124. Yao J, Maslov KI, Zhang Y, Xia Y, Wang LV. Label-free oxygen-metabolic photoacoustic microscopy in vivo. J Biomed Opt. 2011; 16(7):076003. [PubMed: 21806264]

125. Favazza CP, Jassim O, Cornelius LA, Wang LV. In vivo photoacoustic microscopy of human cutaneous microvasculature and a nevus. J Biomed Opt. 2011; 16(1):016015. [PubMed: 21280921]

126. Grootendorst DJ, Jose J, Wouters MW, van Boven H, Van der Hage J, Van Leeuwen TG, et al. First experiences of photoacoustic imaging for detection of melanoma metastases in resected human lymph nodes. Lasers Surg Med. 2012; 44(7):541–9. [PubMed: 22886491]

127. Aizawa K, Sato S, Saitoh D, Ashida H, Obara M. Photoacoustic monitoring of burn healing process in rats. J Biomed Opt. 2008; 13(6):064020. [PubMed: 19123666]

128. Hirao A, Sato S, Saitoh D, Shinomiya N, Ashida H, Obara M. In vivo photoacoustic monitoring of photosensitizer distribution in burned skin for antibacterial photodynamic therapy. Photochemistry and photobiology. 2010; 86(2):426–30. [PubMed: 20074087]

129. Yamazaki M, Sato S, Ashida H, Saito D, Okada Y, Obara M. Measurement of burn depths in rats using multiwavelength photoacoustic depth profiling. J Biomed Opt. 2005; 10(6):064011. [PubMed: 16409076]

130. Zhang HF, Maslov K, Stoica G, Wang LV. Imaging acute thermal burns by photoacoustic microscopy. J Biomed Opt. 2006; 11(5):054033. [PubMed: 17092182]

131. Cancer facts & figures 2009. American Cancer Society; 2009.

132. Shaaban A, Rezvani M. Ovarian cancer: detection and radiologic staging. Top Magn Reson Imaging. 2010; 21(4):247–59. [PubMed: 22082773]

133. Aguirre A, Guo P, Gamelin J, Yan S, Sanders MM, Brewer M, et al. Coregistered three-dimensional ultrasound and photoacoustic imaging system for ovarian tissue characterization. J Biomed Opt. 2009; 14(5):054014. [PubMed: 19895116]

134. Aguirre A, Ardeshirpour Y, Sanders MM, Brewer M, Zhu Q. Potential role of coregistered photoacoustic and ultrasound imaging in ovarian cancer detection and characterization. Transl Oncol. 2011; 4(1):29–37. [PubMed: 21286375]

135. Yang Y, Li X, Wang T, Kumavor PD, Aguirre A, Shung KK, et al. Integrated optical coherence tomography, ultrasound and photoacoustic imaging for ovarian tissue characterization. Biomed Opt Express. 2011; 2(9):2551–61. [PubMed: 21991547]

136. Kumavor PD, Alqasemi U, Tavakoli B, Li H, Yang Y, Sun X, et al. Co-registered pulse-echo/photoacoustic transvaginal probe for real time imaging of ovarian tissue. J Biophotonics. 2013

137. Paterlini-Brechot P. Organ-specific markers in circulating tumor cell screening: an early indicator of metastasis-capable malignancy. Future Oncol. 2011; 7(7):849–71. [PubMed: 21732757]

138. Mavroudis D. Circulating cancer cells. Ann Oncol. 2010; 21(Suppl 7):vii95–100. [PubMed: 20943650]

139. Ireland A, Millward M, Pearce R, Lee M, Ziman M. Genetic factors in metastatic progression of cutaneous melanoma: the future role of circulating melanoma cells in prognosis and management. Clin Exp Metastasis. 2011; 28(4):327–36. [PubMed: 21311956]

140. Mocellin S, Hoon D, Ambrosi A, Nitti D, Rossi CR. The prognostic value of circulating tumor cells in patients with melanoma: a systematic review and meta-analysis. Clin Cancer Res. 2006; 12(15):4605–13. [PubMed: 16899608]

141. Weight RM, Viator JA, Dale PS, Caldwell CW, Lisle AE. Photoacoustic detection of metastatic melanoma cells in the human circulatory system. Opt Lett. 2006; 31(20):2998–3000. [PubMed: 17001379]

142. Gutierrez-Juarez G, Gupta SK, Al-Shaer M, Polo-Parada L, Dale PS, Papageorgio C, et al. Detection of melanoma cells in vitro using an optical detector of photoacoustic waves. Lasers Surg Med. 2010; 42(3):274–81. [PubMed: 20333746]

143. Gutierrez-Juarez G, Gupta SK, Weight RM, Polo-Parada L, Papagiorgio C, Bunch JD, et al. Optical Photoacoustic Detection of Circulating Melanoma Cells In Vitro. Int J Thermophys. 2010; 31(4):784–92. [PubMed: 20730036]

144. McCormack DR, Bhattacharyya K, Kannan R, Katti K, Viator JA. Enhanced photoacoustic detection of melanoma cells using gold nanoparticles. Lasers Surg Med. 2011; 43(4):333–8. [PubMed: 21500228]

145. Weight RM, Dale PS, Viator JA. Detection of circulating melanoma cells in human blood using photoacoustic flowmetry. Conf Proc IEEE Eng Med Biol Soc. 2009; 2009:106–9. [PubMed: 19965119]

146. Zharov VP, Galanzha EI, Shashkov EV, Kim JW, Khlebtsov NG, Tuchin VV. Photoacoustic flow cytometry: principle and application for real-time detection of circulating single nanoparticles, pathogens, and contrast dyes in vivo. J Biomed Opt. 2007; 12(5):051503. [PubMed: 17994867]

147. Galanzha EI, Shashkov EV, Kelly T, Kim JW, Yang L, Zharov VP. In vivo magnetic enrichment and multiplex photoacoustic detection of circulating tumour cells. Nat Nanotechnol. 2009; 4(12): 855–60. [PubMed: 19915570]

148. Nedosekin DA, Sarimollaoglu M, Ye JH, Galanzha EI, Zharov VP. In vivo ultra-fast photoacoustic flow cytometry of circulating human melanoma cells using near-infrared high-pulse rate lasers. Cytometry A. 2011

149. Bhattacharyya K, Goldschmidt BS, Hannink M, Alexander S, Jurkevic A, Viator JA. Gold nanoparticle-mediated detection of circulating cancer cells. Clinics in laboratory medicine. 2012; 32(1):89–101. [PubMed: 22340845]

150. Galanzha EI, Shashkov EV, Spring PM, Suen JY, Zharov VP. In vivo, noninvasive, label-free detection and eradication of circulating metastatic melanoma cells using two-color photoacoustic flow cytometry with a diode laser. Cancer research. 2009; 69(20):7926–34. [PubMed: 19826056]

151. Allen TJ, Hall A, Dhillon AP, Owen JS, Beard PC. Spectroscopic photoacoustic imaging of lipid-rich plaques in the human aorta in the 740 to 1400 nm wavelength range. J Biomed Opt. 2012; 17(6):061209. [PubMed: 22734739]

152. Graf IM, Kim S, Wang B, Smalling R, Emelianov S. Noninvasive detection of intimal xanthoma using combined ultrasound, strain rate and photoacoustic imaging. Ultrasonics. 52(3):435–41. [PubMed: 22078093]

153. Karpiouk AB, Wang B, Emelianov SY. Development of a catheter for combined intravascular ultrasound and photoacoustic imaging. Rev Sci Instrum. 2010; 81(1):014901. [PubMed: 20113121]

154. Wei W, Li X, Zhou Q, Shung KK, Chen Z. Integrated ultrasound and photoacoustic probe for co-registered intravascular imaging. J Biomed Opt. 16(10):106001. [PubMed: 22029348]

155. Hsieh BY, Chen SL, Ling T, Guo LJ, Li PC. Integrated intravascular ultrasound and photoacoustic imaging scan head. Opt Lett. 35(17):2892–4. [PubMed: 20808360]

156. Emelianov S, Wang B, Su J, Karpiouk A, Yantsen E, Sokolov K, et al. Intravascular ultrasound and photoacoustic imaging. Conf Proc IEEE Eng Med Biol Soc. 2008; 2008:2–5. [PubMed: 19162578]

157. Jansen K, van der Steen AF, van Beusekom HM, Oosterhuis JW, van Soest G. Intravascular photoacoustic imaging of human coronary atherosclerosis. Opt Lett. 36(5):597–9. [PubMed: 21368919]

158. Sethuraman S, Aglyamov SR, Amirian JH, Smalling RW, Emelianov SY. Intravascular photoacoustic imaging using an IVUS imaging catheter. IEEE Trans Ultrason Ferroelectr Freq Control. 2007; 54(5):978–86. [PubMed: 17523562]

159. Sethuraman S, Amirian JH, Litovsky SH, Smalling RW, Emelianov SY. Ex vivo Characterization of Atherosclerosis using Intravascular Photoacoustic Imaging. Opt Express. 2007; 15(25):16657–66. [PubMed: 19550952]

160. de la Zerda A, Paulus YM, Teed R, Bodapati S, Dollberg Y, Khuri-Yakub BT, et al. Photoacoustic ocular imaging. Opt Lett. 2010; 35(3):270–2. [PubMed: 20125691]

161. Hu S, Rao B, Maslov K, Wang LV. Label-free photoacoustic ophthalmic angiography. Opt Lett. 2010; 35(1):1–3. [PubMed: 20664653]

162. Song W, Wei Q, Feng L, Sarthy V, Jiao S, Liu X, et al. Multimodal photoacoustic ophthalmoscopy in mouse. J Biophotonics. 2012

163. Song W, Wei Q, Jiao S, Zhang HF. Integrated photoacoustic ophthalmoscopy and spectral-domain optical coherence tomography. J Vis Exp. 2013; (71):e4390. [PubMed: 23354081]

164. Song W, Wei Q, Liu T, Kuai D, Burke JM, Jiao S, et al. Integrating photoacoustic ophthalmoscopy with scanning laser ophthalmoscopy, optical coherence tomography, and fluorescein angiography for a multimodal retinal imaging platform. J Biomed Opt. 2012; 17(6): 061206. [PubMed: 22734736]
165. Jiao S, Jiang M, Hu J, Fawzi A, Zhou Q, Shung KK, et al. Photoacoustic ophthalmoscopy for in vivo retinal imaging. Opt Express. 2010; 18(4):3967–72. [PubMed: 20389409]
166. Sun Y, Sobel ES, Jiang H. First assessment of three-dimensional quantitative photoacoustic tomography for in vivo detection of osteoarthritis in the finger joints. Med Phys. 2011; 38(7): 4009–17. [PubMed: 21858998]
167. Wang X, Chamberland DL, Jamadar DA. Noninvasive photoacoustic tomography of human peripheral joints toward diagnosis of inflammatory arthritis. Opt Lett. 2007; 32(20):3002–4. [PubMed: 17938680]
168. Xiao J, Yao L, Sun Y, Sobel ES, He J, Jiang H. Quantitative two-dimensional photoacoustic tomography of osteoarthritis in the finger joints. Opt Express. 2010; 18(14):14359–65. [PubMed: 20639920]
169. Xu G, Rajian JR, Girish G, Kaplan MJ, Fowlkes JB, Carson PL, et al. Photoacoustic and ultrasound dual-modality imaging of human peripheral joints. J Biomed Opt. 2013; 18(1):10502. [PubMed: 23235916]
170. Hu J, Yu M, Ye F, Xing D. In vivo photoacoustic imaging of osteosarcoma in a rat model. J Biomed Opt. 2011; 16(2):020503. [PubMed: 21361659]
171. Yang X, Wang LV. Monkey brain cortex imaging by photoacoustic tomography. J Biomed Opt. 2008; 13(4):044009. [PubMed: 19021337]
172. Nie L, Cai X, Maslov K, Garcia-Uribe A, Anastasio MA, Wang LV. Photoacoustic tomography through a whole adult human skull with a photon recycler. J Biomed Opt. 2012; 17(11):110506. [PubMed: 23123972]
173. Sussman CB, Rossignol C, Zhang Q, Jiang H, Zheng T, Steindler D, et al. Photoacoustic tomography can detect cerebral hemodynamic alterations in a neonatal rodent model of hypoxia-ischemia. Acta neurobiologiae experimentalis. 2012; 72(3):253–63. [PubMed: 23093012]
174. Kiesslich R, Goetz M, Hoffman A, Galle PR. New imaging techniques and opportunities in endoscopy. Nature reviews Gastroenterology & hepatology. 2011; 8(10):547–53.
175. Zhang JG, Liu HF. Functional imaging and endoscopy. World journal of gastroenterology : WJG. 2011; 17(38):4277–82. [PubMed: 22090783]
176. Yang JM, Favazza C, Chen R, Yao J, Cai X, Maslov K, et al. Simultaneous functional photoacoustic and ultrasonic endoscopy of internal organs in vivo. Nat Med. 2012
177. Yuan Y, Yang S, Xing D. Preclinical photoacoustic imaging endoscope based on acousto-optic coaxial system using ring transducer array. Opt Lett. 2010; 35(13):2266–8. [PubMed: 20596215]
178. Sheaff C, Lau N, Patel H, Huang SW, Ashkenazi S. Photoacoustic imaging endoscope. Conf Proc IEEE Eng Med Biol Soc. 2009; 2009:1983–6. [PubMed: 19964028]
179. Xi L, Grobmyer SR, Wu L, Chen R, Zhou G, Gutwein LG, et al. Evaluation of breast tumor margins in vivo with intraoperative photoacoustic imaging. Opt Express. 2012; 20(8):8726–31. [PubMed: 22513583]
180. Su X, Cheng K, Wang C, Xing L, Wu H, Cheng Z. Image-guided resection of malignant gliomas using fl uorescent nanoparticles. Wiley interdisciplinary reviews Nanomedicine and nanobiotechnology. 2013
181. Grootendorst DJ, Fratila RM, Visscher M, Haken BT, van Wezel RJ, Rottenberg S, et al. Intra-operative ex vivo photoacoustic nodal staging in a rat model using a clinical superparamagnetic iron oxide nanoparticle dispersion. J Biophotonics. 2013; 6(6-7):493–504. [PubMed: 23341267]
182. Cui H, Yang X. In vivo imaging and treatment of solid tumor using integrated photoacoustic imaging and high intensity focused ultrasound system. Med Phys. 2010; 37(9):4777–81. [PubMed: 20964197]
183. Prost A, Funke A, Tanter M, Aubry JF, Bossy E. Photoacoustic-guided ultrasound therapy with a dual-mode ultrasound array. J Biomed Opt. 2012; 17(6):061205. [PubMed: 22734735]

184. Kennedy LC, Bickford LR, Lewinski NA, Coughlin AJ, Hu Y, Day ES, et al. A new era for cancer treatment: gold-nanoparticle-mediated thermal therapies. Small. 2011; 7(2):169–83. [PubMed: 21213377]

185. Su J, Karpiouk A, Wang B, Emelianov S. Photoacoustic imaging of clinical metal needles in tissue. J Biomed Opt. 2010; 15(2):021309. [PubMed: 20459231]

186. Jansen K, van der Steen AF, van Beusekom HM, Oosterhuis JW, van Soest G. Intravascular photoacoustic imaging of human coronary atherosclerosis. Opt Lett. 2011; 36(5):597–9. [PubMed: 21368919]

187. Kim C, Erpelding TN, Jankovic L, Wang LV. Performance benchmarks of an array-based hand-held photoacoustic probe adapted from a clinical ultrasound system for non-invasive sentinel lymph node imaging. Philosophical transactions Series A, Mathematical, physical, and engineering sciences. 2011; 369(1955):4644–50.

188. Yao J, Maslov K, Hu S, Wang LV. Evans blue dye-enhanced capillary-resolution photoacoustic microscopy in vivo. J Biomed Opt. 2009; 14(5):054049. [PubMed: 19895150]

189. Yang Q, Cui H, Cai S, Yang X, Forrest ML. In vivo photoacoustic imaging of chemotherapy-induced apoptosis in squamous cell carcinoma using a near-infrared caspase-9 probe. J Biomed Opt. 2011; 16(11):116026. [PubMed: 22112131]

190. Xiang L, Yuan Y, Xing D, Ou Z, Yang S, Zhou F. Photoacoustic molecular imaging with antibody-functionalized single-walled carbon nanotubes for early diagnosis of tumor. J Biomed Opt. 2009; 14(2):021008. [PubMed: 19405721]

191. de la Zerda A, Bodapati S, Teed R, May SY, Tabakman SM, Liu Z, et al. Family of Enhanced Photoacoustic Imaging Agents for High Sensitivity and Multiplexing Studies in Living Mice. ACS Nano. 2012

192. Akers WJ, Kim C, Berezin M, Guo K, Fuhrhop R, Lanza GM, et al. Noninvasive photoacoustic and fluorescence sentinel lymph node identification using dye-loaded perfluorocarbon nanoparticles. ACS Nano. 2011; 5(1):173–82. [PubMed: 21171567]

193. Xie H, Diagaradjane P, Deorukhkar AA, Goins B, Bao A, Phillips WT, et al. Integrin alphavbeta3-targeted gold nanoshells augment tumor vasculature-specific imaging and therapy. Int J Nanomedicine. 2011; 6:259–69. [PubMed: 21423588]

194. Zhang Q, Iwakuma N, Sharma P, Moudgil BM, Wu C, McNeill J, et al. Gold nanoparticles as a contrast agent for in vivo tumor imaging with photoacoustic tomography. Nanotechnology. 2009; 20(39):395102. [PubMed: 19726840]

195. Lu W, Huang Q, Ku G, Wen X, Zhou M, Guzatov D, et al. Photoacoustic imaging of living mouse brain vasculature using hollow gold nanospheres. Biomaterials. 31(9):2617–26. [PubMed: 20036000]

196. Lu W, Melancon MP, Xiong C, Huang Q, Elliott A, Song S, et al. Effects of photoacoustic imaging and photothermal ablation therapy mediated by targeted hollow gold nanospheres in an orthotopic mouse xenograft model of glioma. Cancer research. 71(19):6116–21. [PubMed: 21856744]

197. Lu W, Xiong C, Zhang G, Huang Q, Zhang R, Zhang JZ, et al. Targeted photothermal ablation of murine melanomas with melanocyte-stimulating hormone analog-conjugated hollow gold nanospheres. Clin Cancer Res. 2009; 15(3):876–86. [PubMed: 19188158]

198. Pan D, Pramanik M, Senpan A, Allen JS, Zhang H, Wickline SA, et al. Molecular photoacoustic imaging of angiogenesis with integrin-targeted gold nanobeacons. FASEB J. 2011; 25(3):875–82. [PubMed: 21097518]

199. Pan D, Pramanik M, Senpan A, Ghosh S, Wickline SA, Wang LV, et al. Near infrared photoacoustic detection of sentinel lymph nodes with gold nanobeacons. Biomaterials. 31(14): 4088–93. [PubMed: 20172607]

200. Homan KA, Souza M, Truby R, Luke GP, Green C, Vreeland E, et al. Silver Nanoplate Contrast Agents for in Vivo Molecular Photoacoustic Imaging. ACS Nano.

201. Wilson K, Homan K, Emelianov S. Biomedical photoacoustics beyond thermal expansion using triggered nanodroplet vaporization for contrast-enhanced imaging. Nat Commun. 3:618. [PubMed: 22233628]

202. Jin Y, Jia C, Huang SW, O'Donnell M, Gao X. Multifunctional nanoparticles as coupled contrast agents. Nat Commun. 1:41. [PubMed: 20975706]

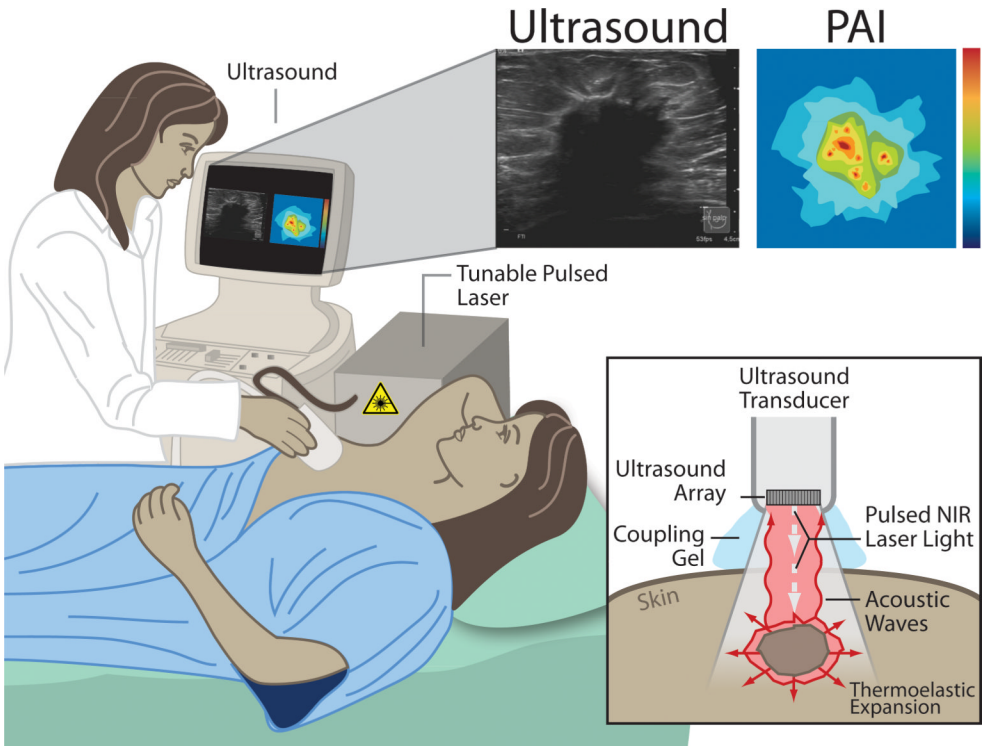

Figure 1.

Principles of photoacoustic imaging (PAI) presented for a potential clinical application: diagnostic breast imaging by integrated real-time photoacoustic/ultrasound imaging. The laser sends nano-second pulses of near-infrared light through the transducer into the tissue. This light is then absorbed inside the tissue (at different levels for each tissue type/component) causing a localized transient thermoelastic expansion. This expansion leads to the emission of pressure waves (ultrasound), which can be detected by the array in the transducer. Finally, a photoacoustic image is calculated and displayed in real-time. At the same time, the ultrasound system can be used in its b-mode to provide structural information about the tissue, in addition to the functional/molecular information obtained by PAI, and both images can be displayed on the view

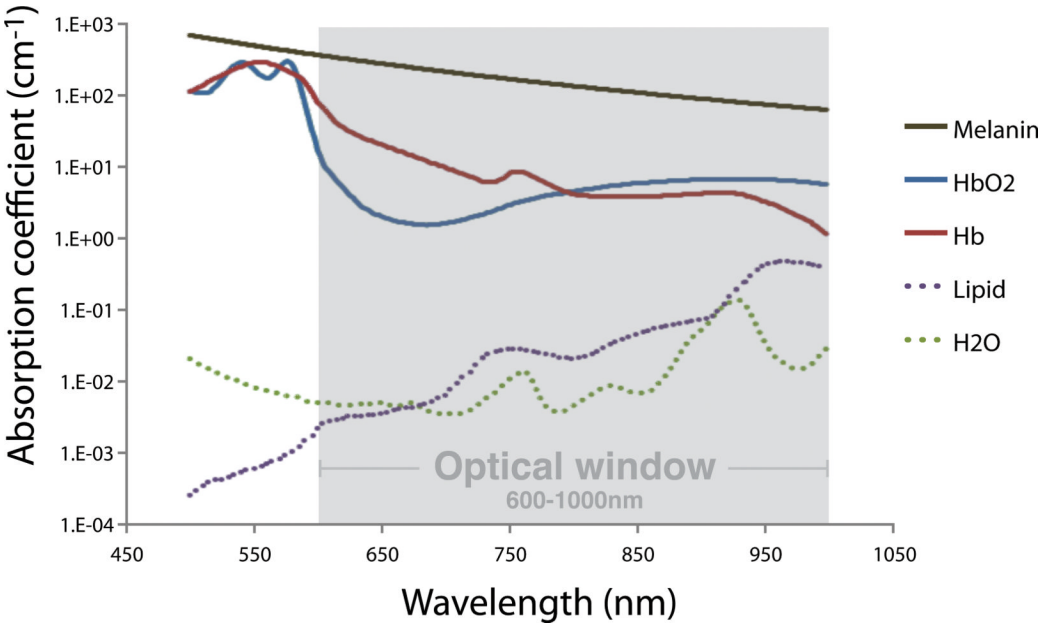

Figure 2.

Absorption spectra of the main light absorbing tissue components: melanin, oxy- and deoxyhemoglobin, lipid, and water. The total light absorbance in these components is lowest in the wavelength range from 600 to 1000 nm. The best tissue penetration depth can thus be reached in this “optical window”. Data obtained from http://omlc.ogi.edu/spectra.

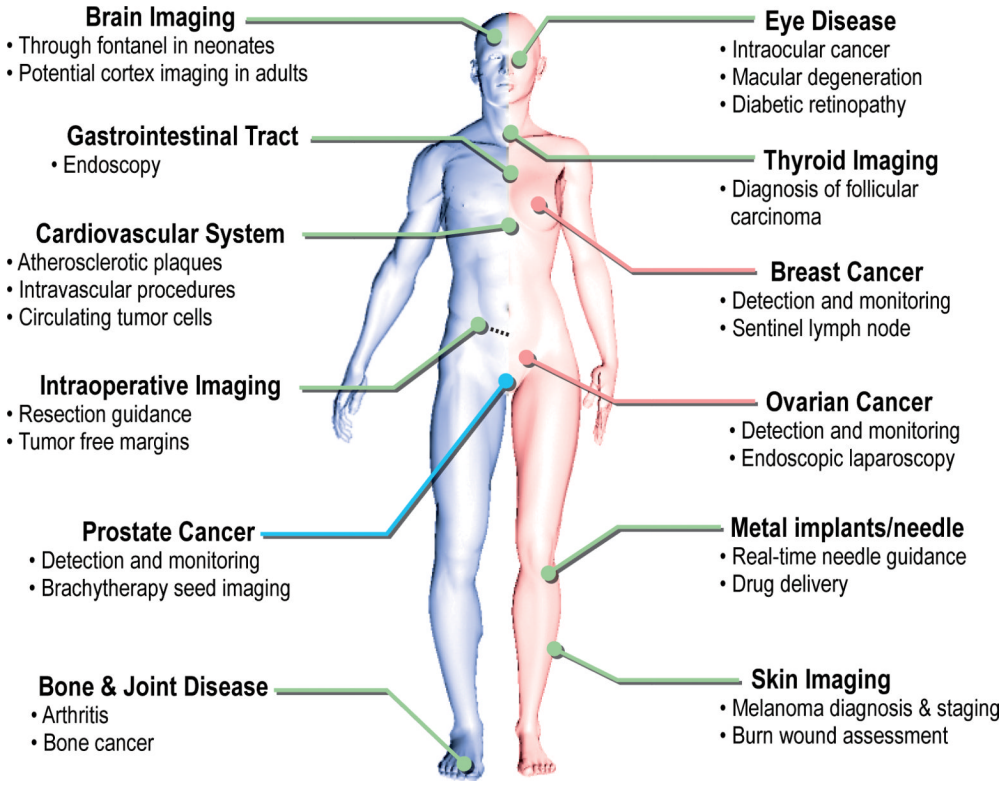

Figure 3.

Overview of potential clinical applications of photoacoustic imaging. For each organ system the main possible applications are listed. Some of these applications are male-specific (left, blue line) and some are female-specific (right, pink line). More detailed information on these clinical applications, the research progress, and challenges can be found in the text under the organ specific sections.

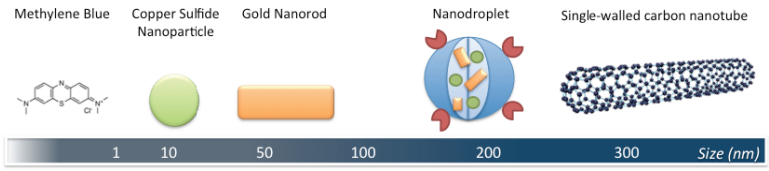

Figure 4.

Illustration of several different types of photoacoustic imaging agents, from small to large (left to right). See Table 1 for more detailed information on these imaging agents. The displayed imaging agents are non-targeted, however, they can all be functionalized by conjugation with specific targeting moieties.

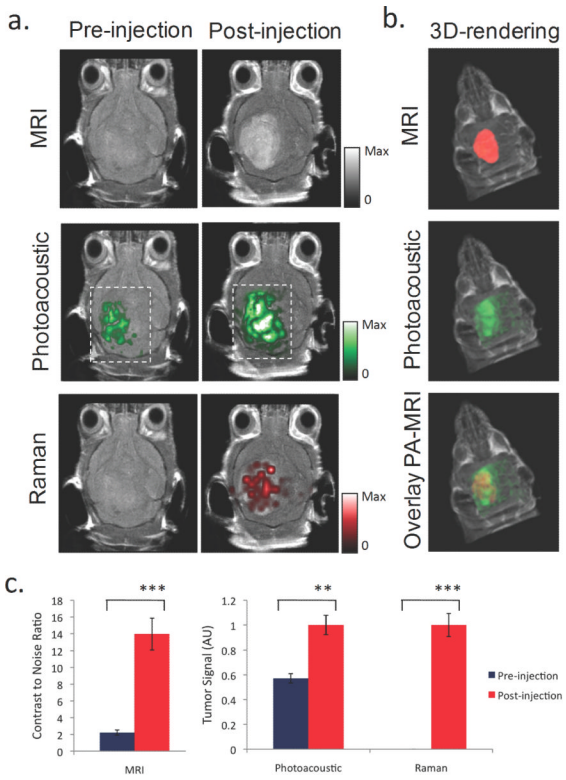

Figure 5.

Triple-modality detection of brain tumors in living mice with MPR nanoparticles. After orthotopic inoculation, tumor bearing mice were injected intravenously with MPR nanoparticles. Photoacoustic, Raman and MRI images of the brain were acquired before and 2 h, 3 h and 4 h post-injection, respectively. a. 2D coronal MRI, Photoacoustic and Raman images. The post-injection images of all three modalities demonstrated clear tumor visualization. The Photoacoustic and Raman images were co-registered with the MRI image, demonstrating good co-localization between the three modalities. b. 3D rendering of MRI image with the tumor segmented in red (top), overlay of MRI and 3D Photoacoustic images (middle) and overlay of MRI, segmented tumor and Photoacoustic image (bottom) showing good co-localization of the Photoacoustic signal with the tumor. c. Quantification of signal in the tumor shows significant increase in MRI, Photoacoustic and Raman signals before versus after the injection ("***" indicates $p < 0.001$, "**" indicates $p < 0.01$). Error bars represent s.e.m. Reprinted by permission from Macmillan Publishers Ltd: Nature Medicine, Kircher MF et al. A brain tumor molecular imaging strategy using a new triple-modality MRI-photoacoustic-Raman nanoparticle. Nat Med. 2012;18(5):829-34, copyright 2012.

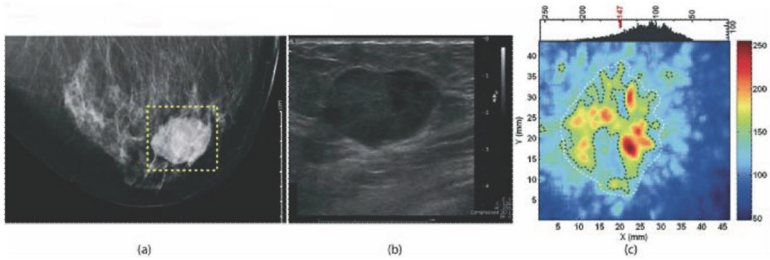

Figure 6.

Photoacoustic imaging study of a suspicious lesion in the right breast of a 57 year old woman that was confirmed to be invasive ductal carcinoma by histopathology. Panel (a) shows the craniocaudal x-ray mammogram of this lesion; panel (b) displays the ultrasound image of the lesion; and panel (c) shows the craniocaudal photoacoustic maximum intensity projection of the same lesion; the higher intensity regions were attributed to tumor vascularization. Reprinted with permission from Manohar et al. Initial results of in vivo non-invasive cancer imaging in the human breast using near-infrared photoacoustics. Opt Express. 2007;15(19):12277-85. Copyright 2007 The Optical Society.

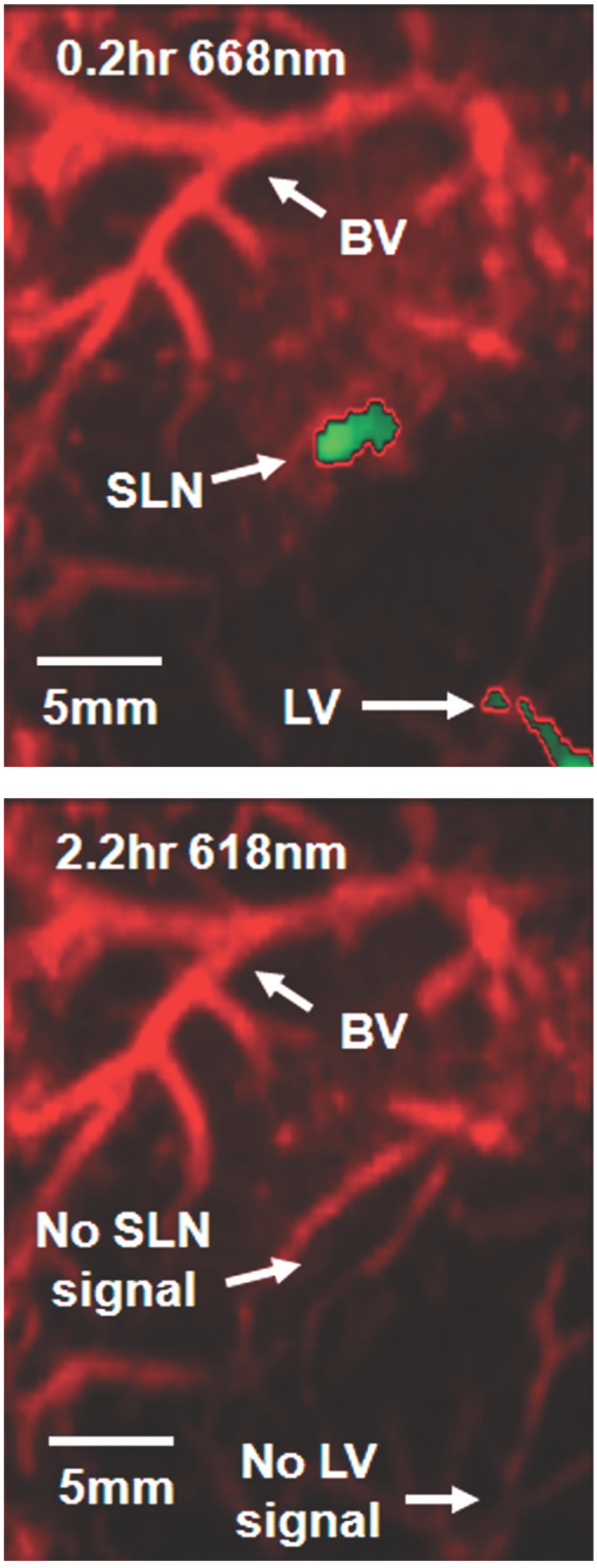

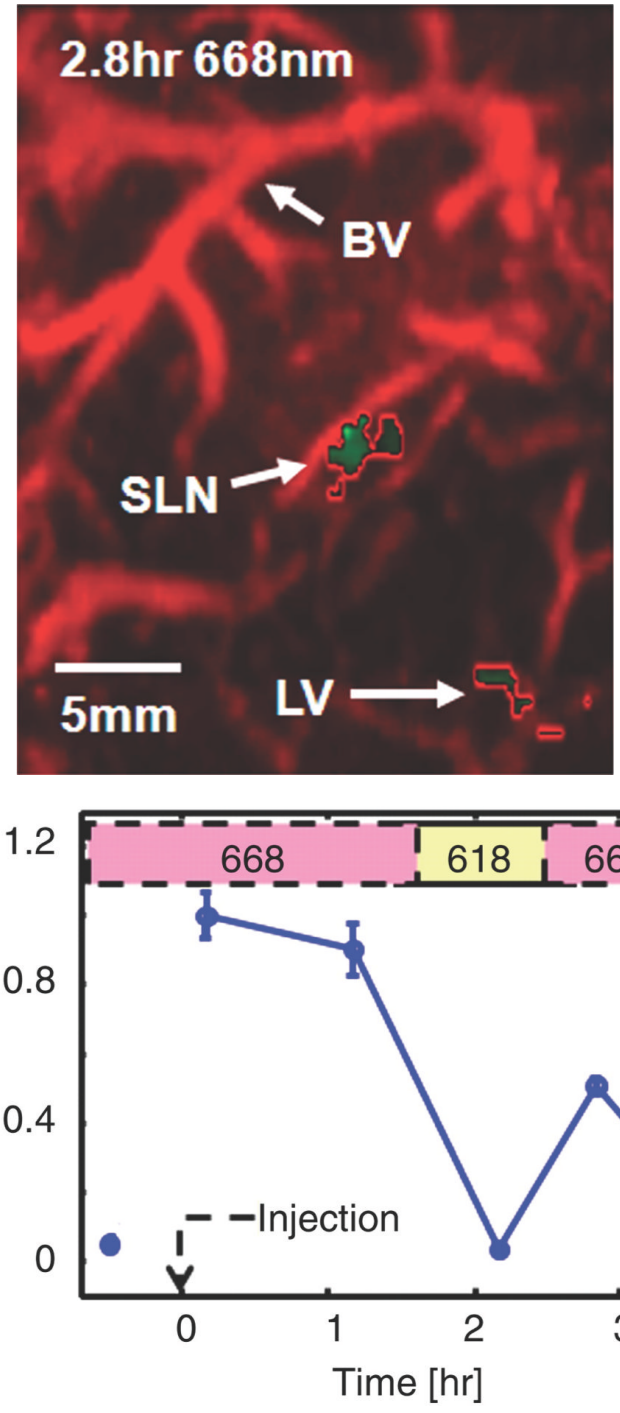

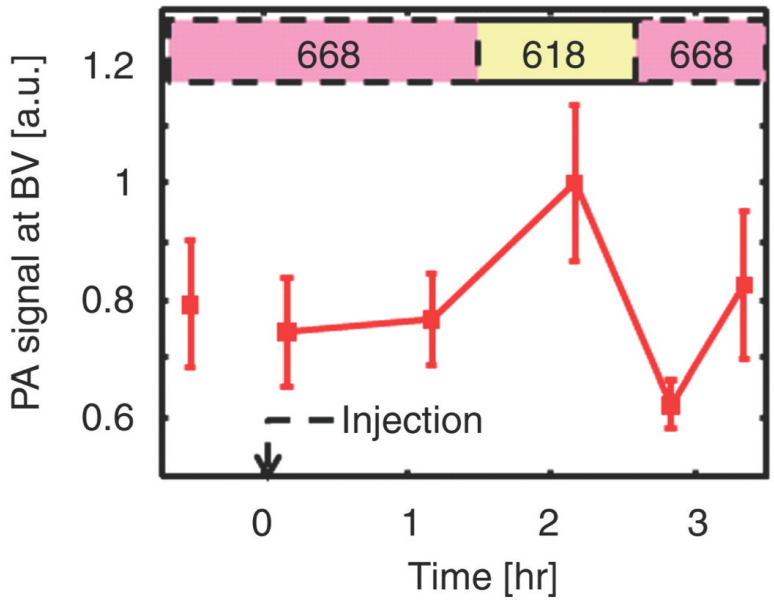

Figure 7.

Photoacoustic images of sentinel lymph node (SLN) in a rat *in vivo* after indocyanine green (ICG) injection. (a) Image at 668 nm 0.2 hour after ICG injection; (b) image at 618 nm 2.2 hours after injection; (c) image at 668 nm 2.8 hours after injection; (d) graph shows comparison of spectroscopic photoacoustic (PA) signals within the SLN region over a period of time; (e) graph shows comparison of spectroscopic photoacoustic signals within blood vessels (BV) over a period of time. LV = lymphatic vessel. Numbers in colored bar at top of d and e = wavelength in nanometers. Reprinted with permission from RSNA (38).

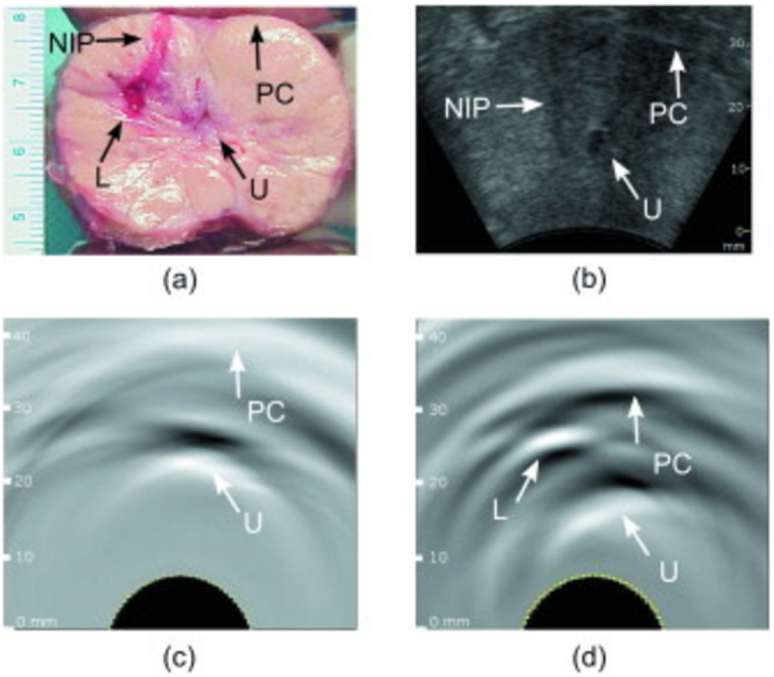

Figure 8.
Photoacoustic imaging study of *ex vivo* dog prostate. Photograph of the sliced prostate (a) shows an induced lesion, (b) shows the ultrasound image of this lesion *in vivo*, (c) and (d) show the *in vivo* photoacoustic images before and after the lesion induction. Prostate capsule (PC), urethra (U), needle insertion path (NIP), and lesion (L) can be distinguished. Reprinted with permission from Yaseen MA et al. Optoacoustic imaging of the prostate: development toward image-guided biopsy. J Biomed Opt. 2010;15(2):021310. Copyright 2010 J Biomed Opt.

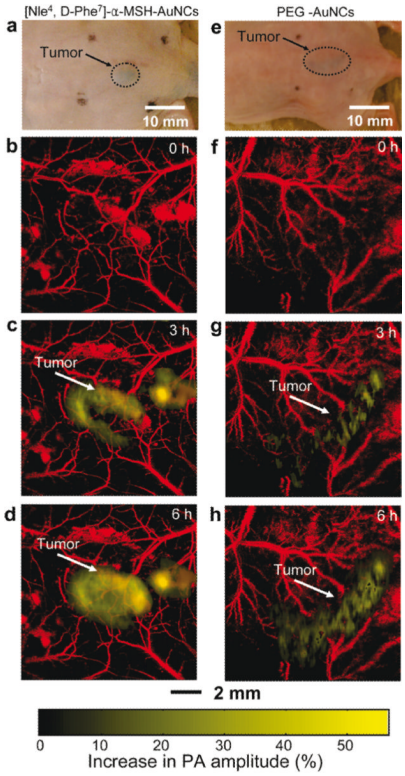

Figure 9.

In vivo noninvasive photoacoustic (PA) time-course coronal maximum amplitude projection (MAP) images of B16 melanomas using targeted [Nle4, D-Phe7]-α-melanocyte-stimulating hormone gold nanocages([Nle4, D-Phe7]-α-MSH-AuNCs) and non-targeted polyethylene glycol gold nanocages (PEG-AuNCs). (a,e) Photographs of nude mice transplanted with B16 melanomas before injection of (a) [Nle4,d-Phe7]-α-MSH- and (e) PEG-AuNCs. Time-course photoacoustic images of the B16 melanomas after intravenous injection with 100 μL of 10 nM (b−d) [Nle4,d-Phe7]-α-MSH- and (f−h) PEG-AuNCs via tail vein. The background vasculature images were obtained at 570 nm (ultrasonic frequency = 50 MHz), and the melanoma images were obtained at 778 nm (ultrasonic frequency = 10 MHz). Color schemes: red for blood vessels and yellow for the increase in PA amplitude. Reprinted with permission from Kim C et al. In vivo molecular photoacoustic tomography of melanomas targeted by bioconjugated gold nanocages. ACS Nano. 2010;4(8):4559-64.). Copyright 2010 American Chemical Society.

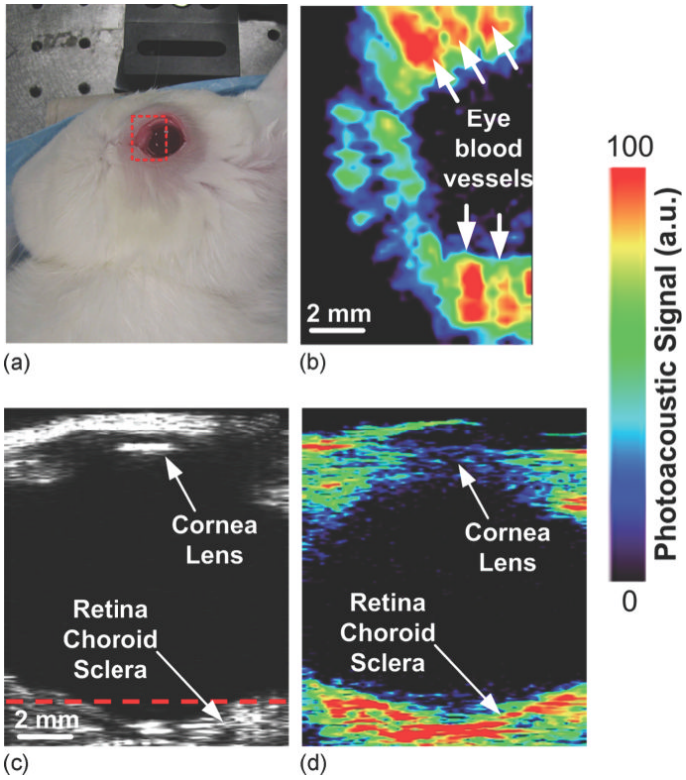

Figure 10.

(a) Photographic, (b) horizontal photoacoustic, (c) vertical ultrasound, and (d) vertical photoacoustic images of an eye of a living rabbit. The area of the eye imaged in (b) is outlined by the red boundary (dotted box) in (a), and the depth is noted by the dashed red line in (c). Reprinted with permission from de la Zerda A, et al. Photoacoustic ocular imaging. Opt Lett. 2010;35(3):270-2. Copyright 2010 Optical Society.

Table 1

Summary of the largest imaging depths reported for macroscopic photoacoustic imaging in experimental and clinical studies.

Depth reached (mm)	Photoacoustic System	Subjects	Target	Imaging agent	Author
Experimental studies					
~ 10	Photoacoustic tomography	Canine prostate *in vivo*	Prostate pseudo lesions with fresh canine blood	-	Wang (112)
~ 20	LOIS-P (Laser Optoacoustic Imaging System for the Prostate)	Dog prostate *in vivo*	Blood rich induced prostate lesions	-	Yaseen (113)
~ 32	Photoacoustic mammascope prototype	Phantom	Breast lesion mimicking objects	Ecoline 700 black water color dye	Manohar (95)
~ 50	Hand-held photoacoustic/ultrasound probe	Phantoms/chicken breast and rats	Sentinel lymph nodes	Methylene Blue	Kim (187)
~ 52	Photoacoustic tomography	Phantoms/chicken breast	Lesion mimicking objects	Blood/Indocyanine Green	Ku (3)
~ 52	Hand-held photoacoustic/ultrasound probe	Phantoms/chicken breast and rats	Sentinel lymph nodes	Methylene Blue	Kim (7)
~ 60	Optoacoustic tomography	Phantoms	Breast cancer cells, HER2	Gold nanoparticles conjugated to Her2-antibody	Copland (52)
~ 70	Thermoacoustic and photoacoustic tomography	Phantoms	Breast lesion mimicking objects	Black India ink	Pramanik (99)
Clinical studies					
~ 28*	Photoacoustic tomography	Patients (n=26)	Breast cancer	-	Kitai (93)
~ 30	LOIS-64 (Laser Optoacoustic Imaging System for the Breast)	Patients (n=27)	Breast cancer	-	Ermilov (31)
~ 30	Photoacoustic mammascope	Patients (n=12)	Breast cancer and cysts	-	Heijblom (94)
~ 40	Photoacoustic tomography	Healthy subject (1)	Breast vasculature	-	Kruger (9)
~ 60	Photoacoustic mammascope	Patients (n=13)	Breast cancer	-	Manohar (8)

*Depth reported for one case only

Table 2

Overview of exogenous photoacoustic molecular imaging agents.

Imaging agent	Type	Size	Absorption wavelength (nm)	Evaluation	Applications	References
Small molecule dyes						
Indocyanine green (ICG)*	Fluorescent dye	< 2 nm	800	Rat model	Brain imaging (angiography), lymph node imaging	Wang (39), Ku (3), Kim (38)
Evans blue*	Fluorescent dye	< 2 nm	550	Mouse and rat model	Imaging microvasculature and lymph nodes	Yao (188), Song (41), Li (42)
IRDye800CW (ICG derivative)	Fluorescent dye	< 2 nm	774	Mouse model	Brain tumor imaging, integrin targeting	Li M (43)
AlexaFluor750	Fluorescent dye	< 2 nm	752	In vitro	Cancer imaging, Her2 targeting	Bhattacharyya (33)
Methylene blue*	Fluorescent dye	< 2 nm	677	Rat model	Lymph node imaging	Song (40)
MMPSense 680	Fluorescent dye	< 2 nm	620; 680	Human endarterectomy specimens	Imaging vulnerability of atherosclerotic plaques, activated by MMPs	Razansky (37)
NIR caspase-9 probe	Fluorescent dye	< 2 nm	640	Mouse model	Monitoring cancer cell apoptosis	Yang (189)
BHQ3	Quencher	< 2 nm	672	In vitro and in vivo in mice	Cancer imaging, thyroid tumors, activated by MMPs	Levi (35, 36)
QXL680	Quencher	< 2 nm	680	In vitro	Cancer imaging, activated by MMPs	Levi (35)
Nanoparticles - nonplasmonic						
Single-walled carbon nanotubes (SWNT) conjugated with targeting peptide	Graphene cylinders	1-2 by 50-300 nm	690	Mouse model	Cancer imaging, integrin targeting	De la Zerda (69), Xiang (190)
SWNT conjugated with ICG and/or QSY and targeting peptide	Graphene cylinders	1-2 by 50-300 nm	780	Mouse model	Cancer imaging, integrin targeting	De la Zerda (68, 191)
SWNT conjugated with ICG	Graphene cylinders	1-2 by 50-300 nm	820	Rat model	Lymph node imaging	Koo (70)
Perfluorocarbon nanoparticles loaded with NIR dyes	Fluorescent dyes encapsulated in perfluorocarbon particles	210-230 nm	790	Rat model	Imaging lymph nodes	Akers (192)
ICG-embedded PEBBLEs	Fluorescent dye encapsulated in ormosil spheres	100 nm	790	Mouse model	Cancer imaging, Her2 targeting	Kim (44)

Imaging agent	Type	Size	Absorption wavelength (nm)	Evaluation	Applications	References
ICG encapsulated in virus-mimicking nano-constructs	Fluorescent dye encapsulated in protein shell, purified from virus	30 nm	760-820	Phantoms	Photoacoustic imaging	Gupta (45)
Quantum dots	Fluorescent	2-10 nm	640	In vitro	Photoacoustic imaging	Shashkov (72)
Copper Sulfide nanoparticles	Copper sulfide spheres	11 nm	1064	Mouse and rat model	Brain and lymph node imaging	Ku (73)
Nanoparticles - plasmonic						
Gold nanocages	Silver cubes coated with a layer of gold	40 nm	800	Mouse and rat model	Brain imaging (angiography), melanoma imaging	Skrabalak (54), Yang (55), Kim (53)
Gold nanoshells	Spherical particles with silica core and gold shell	100-200 nm	800	Mouse and rat model	Cancer imaging, colon and brain cancer, integrin targeting	Xie (193), Li (26)
Gold nanorods	Solid gold rice-shaped particles	10 by 40-60 nm	650-1100	Mouse model	Cancer imaging, Her2 and EGFR targeting	Eghtedari (49, 50), Copland (52), Li (46), Bayer (46), Jokerst (57)
Silica-coated gold nanorods	Solid gold rods coated with silica layer	60-70 by 80-90 nm	665	Mouse model	Mesenchymal stem cell imaging	Jokerst (56)
Gold nanospheres	Solid gold spheres	20-50 nm	520-530	Mouse model	Cancer imaging	Zhang (194)
Hollow gold nanospheres	Spheres with hollow core and gold shell	50 nm	800	Mouse model	Brain vasculature and tumor imaging, melanoma targeting	Lu (195-197)
Gold nanobeacons	Liposomes containing plasmonic nanoparticles	100-200 nm	520-1100	Mouse model	Cancer imaging, integrin targeting, lymph node imaging	Pan (198, 199)
Gold nanoclusters	4-nm gold spheres connected with biodegradable polymer	50-100 nm	700-900	Phantoms	Imaging with high clearance	Yoon (62)
SWNT with gold coating	Gold coated grapheme cylinders	11 by 100 nm	850	Mouse model	Imaging lymphatic vessels	Kim (71)
Fluorescent nanodiamonds conjugated with gold nanoparticles	Diamond nanocrystallites linked to gold particles	150-250 nm	530, 565	In vitro	Photoacoustic imaging	Zhang (65)
Radiation-damaged nanodiamonds	Nanodiamonds irradiated with 40 keV Helium ions	70 nm	820	Mouse model	Photoacoustic imaging	Zhang (66)
Silver nanoplates	Triangular silver plates	10-30 by 25-250 nm	550 - 1080	Mouse model	Cancer imaging, targeting EGFR	Homan (200)

Imaging agent	Type	Size	Absorption wavelength (nm)	Evaluation	Applications	References
Multimodality imaging agents						
MPR nanoparticle	Gold core with Raman active layer and silica shell coated with gadolinium	120-180 nm	540	Mouse model	Imaging brain tumors with three modalities: MRI, PAI, and Raman imaging	Kircher (86)
Photoacoustic nanodroplets	Droplets of perfluorocarbon loaded with optically absorbing nanoparticles	200 nm	520-1200	Mouse model	Optically triggered dual-contrast imaging for photoacoustic and ultrasound imaging	Wilson (201)
Radiolabled gold nanorods	Gold nanorods labeled with ^{125}I	10 by 40-60 nm	650-1100	Rat model	Dual mode PAI and SPECT in rat tail joints	Agarwal (85)
Pearl necklaces	Gold nanorods decorated with iron oxide spheres	90 nm	785	In vitro	Dual mode cancer imaging with PAI and MRI	Wang (80)
Nanostars	Iron oxide cores with gold spikes	120 nm	800-900	Rat model	Imaging lymphatic vessels and nodes	Kim (58)
Nanoroses	Clusters of iron oxide cores with thin knobby gold coating	20-80 nm	700-800	In vitro and rabbit model (atherosclerosis)	Cancer imaging, EGFR targeting; atherosclerosis imaging	Ma (59, 60)
Nanowontons	Wonton-shaped cobalt cores coated with layer of gold	30-90 nm	400-800	Phantoms and mouse model	Dual mode PAI and MRI	Bouchard (61)
Iron oxide-gold nanoshells	Iron oxide cores with gold shells	30-40 nm	600-900	Phantoms	Dual mode PAI and MRI	Jin (202)
Superparamagnetic iron oxide nanoparticles	Iron oxide cores embedded in dextran coating	80-150 nm	720	Rat model - ex vivo	Photoacoustic intra-operative lymph node imaging with MRI imaging agent	Grootendorst (87)
Magneto-plasmonic nanoparticles	liposomes encapsulating gold nanorods and iron oxide spheres	100-200 nm	800	Phantoms	Dual mode PAI and MRI	Qu (82)

MMP: matrix metalloproteinase; ICG: indocyanine green; EGFR: epidermal growth factor receptor; Her2: human epidermal growth factor receptor 2; PAI: photoacoustic imaging; MRI: magnetic resonance imaging; SPECT: single photon emission computed tomography; NIR: near-infrared

*FDA approved